The Astrophysical Journal, 926:131 (18pp), 2022 February 20 https://doi.org/10.3847/1538-4357/ac469f

The Environments of Green Pea Galaxies. I. The KISS Sample

Samantha W. Brunker[1], John J. Salzer[1], Brooke Kimsey-Miller[1], and Bryce Cousins[2,3]
[1] Department of Astronomy, Indiana University, 727 East Third Street, Bloomington, IN 47405, USA; sbrunker@indiana.edu
[2] Department of Physics, The Pennsylvania State University, University Park, PA 16802, USA
[3] Institute for Gravitation and the Cosmos, The Pennsylvania State University, University Park, PA 16802, USA
Received 2021 September 23; revised 2021 November 20; accepted 2021 December 22; published 2022 February 18

Abstract

We present environmental analyses for 13 KPNO International Spectroscopic Survey Green Pea (GP) galaxies. These galaxies were discovered via their strong [O III] emission in the redshift range $0.29 < z < 0.42$, and they are undergoing a major burst of star formation. A primary goal of this study is to understand what role the environment plays in driving the current star formation activity. By studying the environments around these extreme star-forming galaxies, we can learn more about what triggers their star formation processes and how they fit into the narrative of galaxy evolution. Using the Hydra multifiber spectrograph on the WIYN 3.5 m telescope, we mapped out the galaxy distribution around each of the GPs (out to ∼15 Mpc at the redshifts of the targets). Using three density analysis methodologies chosen for their compatibility with the geometry of our redshift survey, we categorized the galaxian densities of the GPs into different density regimes. We find that the GPs in our sample tend to be located in low-density environments. We find no correlation between the density and the SFRs seen in the GPs. We conclude that the environments the GPs are found in are likely not the driving factor behind their extreme star formation activity.

Unified Astronomy Thesaurus concepts: Emission line galaxies (459); Starburst galaxies (1570); Star formation (1569); Galaxy environments (2029); Redshift surveys (1378)

1. Introduction

Green Pea galaxies (GPs) are extreme star-forming galaxies. They are typically found to be compact and have low metallicities and very high specific star formation rates (e.g., Izotov et al. 2011; Nakajima & Ouchi 2014; Henry et al. 2015). GPs were originally discovered by citizen scientists as part of the Galaxy Zoo galaxy classification project. Following this discovery, Cardamone et al. (2009) published the first sample of GPs that were selected from the Sloan Digital Sky Survey (SDSS; York et al. 2000). Due to their color selection, GP galaxies are generally found at intermediate redshifts, $0.141 < z < 0.348$ (Cardamone et al. 2009), but there are GP-like galaxies being discovered at even higher redshifts. The Cardamone et al. (2009) GPs range in mass from $10^{8.5}$ to $10^{10.5}\,M_{\odot}$, making them significantly more massive than the dwarf starbursting galaxies seen in the local universe (i.e., Blue Compact Dwarfs (BCDs)). GPs are quite rare, and we do not see any other class of galaxies in the local universe that have properties as extreme as those of the GPs.

Recently GPs have become a prime target for studying the contribution from star-forming galaxies during the epoch of reionization. Many GPs have been observed to leak ionizing Lyman continuum radiation (e.g., Henry et al. 2015; Izotov et al. 2016a, 2016b, 2017; Jaskot et al. 2017; Verhamme et al. 2017; Yang et al. 2017a; Izotov et al. 2018), so there is great interest in studying them closely to better understand the sources of ionizing radiation and how that radiation escapes from galaxies. The GPs are believed to have properties similar to early galaxies from the epoch of reionization, so they are generally thought of as low-redshift analogs (e.g., Lofthouse et al. 2017; Kim et al. 2021).

Despite the intense interest in using the GPs as analogs for high-redshift star-forming galaxies, we do not have a good understanding of what is actually going on in the GPs themselves. Specifically, we do not understand why the GPs are going through such an extreme star-forming event. The compact nature of the GPs as well as their distances from us make it difficult to study their internal structure and their immediate environments.

The primary goal of this study is to understand what role the environment plays in driving the current star formation activity. Understanding what triggered the current star formation event in the GPs should allow us to better understand the evolutionary status and possibly the formation scenarios of the GPs. Generally, the environment a galaxy lives in can play a large role in its star formation history. Galaxy interactions and mergers are known triggers of star formation (e.g., Barton et al. 2000; Lambas et al. 2003; Brosch et al. 2004; Barton et al. 2007; Li et al. 2008). In this study, we focus on studying the environments around the sample introduced in Brunker et al. (2020), in order to determine what kinds of environments GPs are found in, and whether that environment is likely to have played a role in triggering the ongoing star formation events in the GPs.

Previously, Kurtz et al. (2016) presented a study of GP environments. Their study included GPs at the lower redshift end of the GP redshift distribution in order to take advantage of the existing SDSS redshift data. They found GPs in a wide variety of environments ranging from low-density environments to galaxy clusters. Yang et al. (2017b) also analyzed the environments around their sample of Blueberry galaxies using nearest neighbor distances calculated from the SDSS spectroscopic catalog. They found that Blueberries are generally found in low-density environments, and some are found on the outskirts of galaxy groups.

In this paper, we present the results of an extensive redshift survey of 13 GP fields as well as the environmental analyses of

Table 1
KISSR Green Peas—Properties

KISSR	R.A. degrees	Decl. degrees	z	$EW_{[O\ III]}$ Å	M_B	$\log(M_*)$ $M_\odot$	log(O/H)+12	log(SFR) $M_\odot\ yr^{-1}$
(1)	(2)	(3)	(4)	(5)	(6)	(7)	(8)	(9)
225	197.54067	29.29527	0.35822	102.4	−21.61	9.73	8.58	1.61
560	217.45028	29.48553	0.35787	405.7	−19.95	8.99	7.80	0.80
847	235.98020	29.46394	0.35575	1896.0	−19.52	8.86	7.65	1.36
1038	247.14056	29.32112	0.41001	731.1	−21.20	9.69	8.20	1.63
1290	185.60078	43.18965	0.30496	272.7	−20.89	9.44	8.25	0.97
1508	198.67200	43.72399	0.29397	413.1	−21.02	9.55	8.30	1.01
1516	198.95600	43.57503	0.32766	685.6	−21.69	9.67	8.17	1.32
1759	215.15889	43.72554	0.40504	1129.0	−19.95	9.32	7.97	1.02
1791	217.42047	43.90243	0.35923	213.1	−21.00	10.15	8.41	1.37
1825	219.08469	43.88378	0.33112	155.5	−21.67	10.25	8.60	1.26
1953	231.59900	43.00455	0.36882	427.2	−21.58	9.62	8.20	1.42
2005	235.69358	43.89937	0.30805	345.1	−21.03	9.10	8.46	1.31
2042	237.44008	43.05719	0.35680	953.2	−20.42	8.98	7.77	1.14

Note. Uncertainties for the stellar masses (column 7) are 0.2–0.3 dex; uncertainties for the metallicities (column 8) are 0.10–0.15 dex; typical uncertainties in the SFRs (column 9) are ∼10%.

these GPs. The sample selection and the description of the observations for the redshift survey are presented in Section 2. A summary of the various density analyses we performed for each GP field are presented in Section 3. In Section 4, we present the results of our environmental analysis for each GP field specifically, and we discuss the environmental analysis results for the GPs as a group. Our findings are summarized in Section 5.

2. KISS GP Redshift Survey

To investigate the environments of the KPNO International Spectroscopic Survey (KISS) red (hereafter KISSR) GPs we designed and completed our own redshift survey of galaxies located in the same fields as the KISSR GPs. We decided to pursue this avenue of work because there was not much redshift data available for galaxies in the same redshift range as our GPs. This data set allows us to study the effects of the GP environments on their star formation activity.

2.1. Sample Selection

2.1.1. Green Pea Galaxies

The GP galaxies being studied in the current paper were discovered in KISS (Salzer et al. 2000). KISS employed a low-dispersion objective prism on the 0.61 m Burrell Schmidt[4] telescope on Kitt Peak to carry out a comprehensive survey of emission-line galaxies (ELGs) in the nearby universe. The objective-prism spectra covered two distinct wavelength ranges: $\lambda\lambda$ 6400–7200 Å (KISSR, selected primarily by the Hα line; Salzer et al. 2001; Gronwall et al. 2004b; Jangren et al. 2005a) and $\lambda\lambda$ 4800–5500 Å (KISS blue, selected primarily by the [O III]λ5007 line; Salzer et al. 2002). A program of "quick-look" follow-up spectroscopy was carried out by members of the KISS collaboration (Wegner et al. 2003; Gronwall et al. 2004a; Jangren et al. 2005b; Salzer et al. 2005). All 2157 KISSR ELGs from the first two survey catalogs (Salzer et al. 2001; Gronwall et al. 2004b, hereafter KR1 and KR2, respectively) possess follow-up spectra.

The vast majority of KISSR galaxies were detected via the Hα emission line, resulting in a sample of ELGs with redshifts between 0.0 and 0.095 (limited by the survey filter). However, roughly 2% were detected by strong [O III]λ5007 emission that was redshifted into the KISSR filter bandpass. These objects, which have redshifts between 0.29 and 0.42, tend to have large equivalent width emission lines and high excitation (large [O III]/Hβ) values.

In a preliminary analysis, Salzer et al. (2009) found that 15 of the 38 [O III]-detected KISSR ELGs were star-forming systems based on their locations in line diagnostic diagrams (e.g., Baldwin et al. 1981; Veilleux & Osterbrock 1987); the remaining [O III]-detections were all AGNs, mainly Seyfert 2 galaxies. Two of the star-forming [O III]-detected KISSR galaxies (KISSR 169 and 980) do not have characteristics that mimic the GP galaxies and will not be discussed further. See Brunker et al. (2020) for more details.

In Brunker et al. (2020), we characterized properties of the 13 KISSR [O III]-detected star-forming ELGs, and the observed and derived characteristics of the KISSR GPs are presented in Table 1. Column 1 lists the KISSR number, while columns 2 and 3 give the equatorial coordinates of our galaxies (J2000). The measured redshifts and [O III] equivalent widths, derived from the KISS quick-look spectra, are given in columns 4 and 5. Formal uncertainties in the KISSR photometric and spectroscopic quantities listed here are included in the survey papers cited above. B-band absolute magnitudes are listed in column 6. These are observed, as opposed to rest-frame (i.e., K corrected), luminosities. Typical uncertainties are 0.1–0.2 mag. The stellar masses are listed in column 7. These values were derived as described in Brunker et al. (2020) and have typical uncertainties of 0.2–0.3 dex in $\log(M_*)$ (30%–50% uncertainties in mass). Oxygen abundances are listed in column 8. These values are derived using the O3N2 strong-line method and have uncertainties of 0.10–0.15 dex (Hirschauer et al. 2018). Improved metallicities obtained using the direct method will be presented in S. W. Brunker et al. (2022, in preparation). Column 9 presents the star formation rates (SFRs). These are derived using the Hα line fluxes and employ the standard Kennicutt (1998) SFR conversion factor ($SFR = L_{H\alpha} \cdot 7.9 \times 10^{-42}$). Typical uncertainties in the SFR values are ∼10%, where the error is dominated by the uncertainty in the distance.

[4] The Burrell Schmidt telescope of the Warner and Swasey Observatory is operated by Case Western Reserve University.

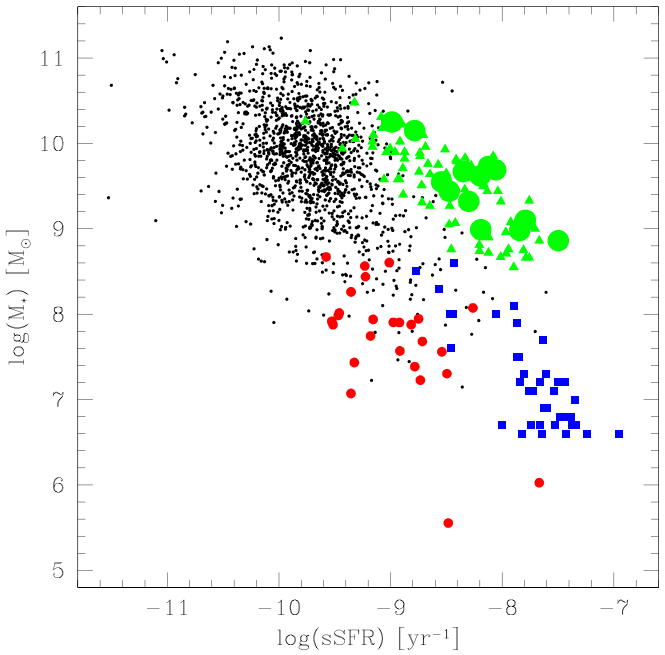

Figure 1. Five distinct samples of star-forming galaxies are shown in this plot of stellar mass (M_*) vs. specific star formation rate (sSFR). The following galaxy catalogs are included: the Cardamone et al. (2009) GPs are shown as green triangles, the KISSR GPs are plotted as large green circles, the Yang et al. (2017b) Blueberries are given as blue squares, a sample of BCDs from Hirschauer et al. (2022) are shown as red dots, and the full sample of KISSR star-forming galaxies (Salzer et al. 2001; Gronwall et al. 2004b) are indicated by black dots. The two GP samples are seen to overlap completely. The "extreme" star-forming galaxies (GPs, BCDs, and Blueberries) are seen to segregate themselves from the more generic KISSR sample of star-forming galaxies. The BCDs and Blueberries are confined to low-mass systems, as expected, with the Blueberries distinguishing themselves by their extreme sSFRs. The GPs, by contrast, are found in intermediate and high-mass galaxies, and are clearly offset to higher values of sSFR when compared to the KISSR star-forming galaxies of similar mass.

The KISSR GPs were compared with the original GP galaxy sample from Cardamone et al. (2009) in Brunker et al. (2020). The 13 KISSR [O III]-detected star-forming galaxies overlapped with the Cardamone et al. (2009) sample completely in terms of their luminosities, stellar masses, oxygen abundances, star formation rates, and [O III] equivalent widths. That study concluded that the KISSR [O III]-detected galaxies were *bona fide* GPs; we will refer to them as GPs going forward. These 13 KISSR GPs are located at the centers of the fields we observed for this environment study.

To help put the GPs into context, we compare their locations in the stellar mass (M_*)—specific star formation rate (sSFR) plane in Figure 1. Four different samples of "extreme" star-forming galaxies are included in the figure: the GPs of Cardamone et al. (2009) (green triangles) and Brunker et al. (2020) (i.e., the current sample; green circles), the Blueberry galaxies from Yang et al. (2017b) (blue squares), and a sample of BCDs drawn from the Hα Dot survey (Kellar et al. 2012; Salzer et al. 2020) that are included in a study by Hirschauer et al. (2022) (red dots). The small black dots represent a more generic sample of star-forming galaxies from the KISSR (Salzer et al. 2001; Gronwall et al. 2004b).

There are several relevant points that can be drawn from from inspection of Figure 1. First, it is important to note that the selection methods for each of these samples is distinctly different; the segregation of the four "extreme" star-forming galaxy samples from each other is primary caused by selection effects. For example, the redshift ranges of the GPs, Blueberries, and BCDs plotted do not overlap, and the survey methods employed to catalog the GPs and Blueberries are such that these surveys could *only* find the most extreme galaxies present in the survey volume.

Comparison of the two GP samples in Figure 1 shows essentially complete overlap despite the very different selection methods employed to detect them (color selection versus objective-prism emission-line detection). This supports the contention made above that the KISSR [O III]-detected galaxies are *bona fide* GPs. Next, we point out the mass distributions of the "extreme" systems. The BCDs and Blueberries are all found at lower masses: they are true dwarf galaxies. On the other hand, the GPs are seen to possess intermediate and high masses. There is very little overlap in the mass ranges of the three groups. Finally, this figure illustrates nicely the extreme magnitude of the star-forming events going on in GP galaxies. The GPs in the lower right end of their grouping in Figure 1 have sSFR values comparable to the most extreme Blueberries despite being 2 orders of magnitude more massive.

2.1.2. Redshift Survey Sample

To find galaxy targets for our environment survey, we used the SDSS. Though the spectroscopic component of the SDSS does not go deep enough to include spectra of many galaxies in the redshift range of each KISSR GP, we used the SDSS to compile lists of galaxies within 30′ of each target that have magnitudes brighter than $g = 21$. Once we had a list of all the galaxies in this field of view around the KISSR GP, we refined the target lists using the SDSS-derived photometric redshifts. Though the photometric redshifts have a large uncertainty, we used them as a rough selection criterion in order to pick out galaxies most likely to be in the redshift range of our KISSR GPs.

We created two target lists consisting of "bright" and "faint" targets. For the bright targets, we selected galaxies with photometric redshifts within ±0.1 of the redshifts of the KISSR GPs. For the faint targets, we selected all galaxies within ±0.05 of the redshifts of the KISSR GPs. Additionally for the faint targets, we selected galaxies within a 10' radius of the KISSR GPs that have photometric redshifts within ±0.1 of the redshifts of the KISSR GPs to add to the already selected targets. We added this additional step for the faint targets to ensure we primarily focused on targets close to the KISSR GPs on the sky since we want to study their immediate environments. This selection is illustrated for the KISSR 1791 field in Figure 2. The red vertical line shows the separation between the bright and faint targets. The red horizontal lines show the photometric redshift cuts for the galaxies in the full field of view, and the blue horizontal lines indicate the additional target selection for the faint galaxies within a 10′ radius of the KISSR GPs.

2.2. Observations

In order to measure the redshifts of galaxies along the line of sight of our KISSR GPs, we used the Hydra multifiber positioner and the Bench Spectrograph on the WIYN 3.5 meter telescope. [5] The fields of view of WIYN and Hydra allow us to map galaxies in the fields of our KISSR targets out to 30′ from

[5] The WIYN Observatory is a joint facility of the NSF's National Optical–Infrared Astronomy Research Laboratory, Indiana University, the University of Wisconsin-Madison, Pennsylvania State University, the University of Missouri, the University of California-Irvine, and Purdue University.

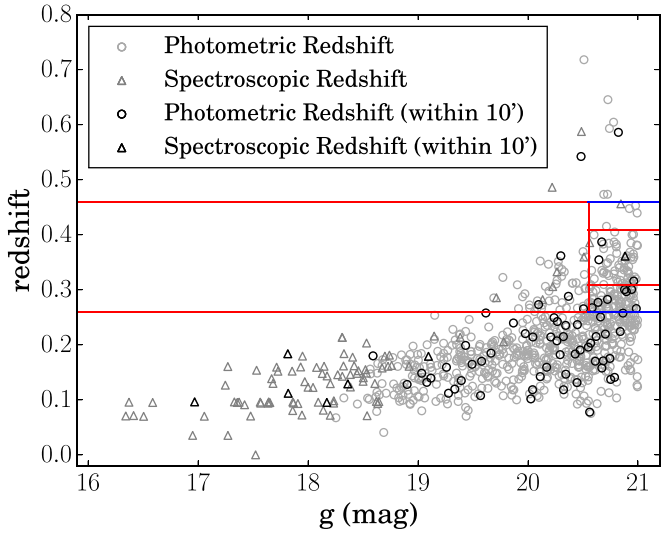

Figure 2. The redshift survey target selection process is illustrated for the KISSR 1791 field. The gray points are galaxies from the SDSS within a 30′ radius around KISSR 1791 with magnitudes brighter than $g = 21$. The triangles are galaxies with measured spectroscopic redshifts in the SDSS, and the circles are galaxies that only have photometric redshifts. The black points indicate which galaxies are within a 10′ radius around KISSR 1791. The vertical red line at a g magnitude of 20.55 indicates the separation between the "bright" and "faint" target lists created. For the bright targets, galaxies with photometric redshifts (circles) within ±0.1 of the redshift of KISSR 1791 ($z = 0.35923$) were selected. This selection region is shown by the horizontal red lines. For the faint targets, galaxies with photometric redshifts within ±0.05 of the redshift of KISSR 1791 were selected, also indicated by horizontal red lines. Additionally, in the faint sample, we also selected galaxies within a 10′ radius of KISSR 1791 between ±0.05 and 0.1 of the redshift of KISSR 1791 (black circles between the horizontal red and blue lines).

the central GP. At the redshifts of the KISSR GPs ($\langle z \rangle = 0.35$), this corresponds to ∼14 Mpc and is large enough to trace the large-scale structure around the KISS GPs as well as the immediate environment around the GPs.

We observed KISSR GP fields with multiple configurations in order to observe a significant amount of our SDSS target galaxies. Each fiber configuration was observed for a total of 1.5 hr in a series of three 30 minute exposures. This helps reduce the effects of cosmic rays in the final combined spectra. We used the red-sensitive fibers on Hydra because the fiber size (2") is well matched with the sizes of the SDSS targets and because of the superior transmission characteristics. By observing multiple configurations for each GP field, we were partly able to overcome the observing limitations including the minimum fiber separation (37″) and locations of broken fibers. The wavelength range of our observations is $4600 \lesssim \lambda \lesssim 7400$, which covers from the [O II]$\lambda\lambda$ 3726,29 doublet out to the [O III]λ5007 line at the redshifts of our KISS GPs.

Hydra fibers were always placed on the central KISS GP in each field to obtain their spectra. Quick-look spectra were previously obtained for these galaxies in order to identify them as [O III]-selected KISS galaxies, but the quality of the quick-look spectra were not enough to measure T_e (direct) abundances. T_e abundances are derived from measurements of temperature-sensitive line ratios, i.e., [O III]$\lambda\lambda$ 4959,5007/[O III]λ4363. The [O III]λ4363 line can be very weak and difficult to measure. The WIYN Hydra spectra for the KISS targets are higher quality than the quick-look spectra, and the auroral [O III]λ4363 line is measurable in a majority of the KISS GPs. This allows us to determine much more accurately the abundances of these KISS target galaxies. Our abundance analysis will be presented in a separate study (S. W. Brunker et al. 2022, in preparation).

The Hydra spectra were reduced using the Image Reduction and Analysis Facility (IRAF) software package. Processing of the 2D spectral images followed standard methods. The scattered light subtractions, extraction, flat-fielding, fiber throughput corrections, wavelength calibrations with CuAr comparison lamp spectra, and sky subtractions were completed using the DOHYDRA routine in IRAF. In order to determine the redshifts of the galaxies around the KISS GPs, we used two methods.

For galaxies with emission-line features, we were able to use the spectral analysis package WRALF (WRapped Automated Line Fitting; Cousins 2019) which was developed to automate the process of measuring emission lines in star-forming galaxies. WRALF is a Python package which uses the Fortran code ALFA (Automated Line Fitting Algorithm; Wesson 2016) to identify and classify emission lines in galaxy spectra by performing Gaussian line-fitting for each emission line in a spectrum. ALFA then estimates redshift and line fluxes (Wesson 2016). WRALF uses this information to compute the reddening coefficients and reddening-corrected line ratios for each galaxy. Using WRALF we were able to measure the redshifts for all of the galaxies in our sample that contained emission lines. Because WRALF only requires the user to identify a single emission line in each galaxy spectrum, it greatly reduced the time it took to analyze a significant amount of our data compared with manually measuring emission lines.

For galaxies which had no emission line features and only had absorption features, we used FXCOR, a cross correlation package in IRAF to measure the redshifts. We used three template spectra of galaxies with strong, clear absorption line features and no emission line features from our observations where the redshift was measured by hand, and these were then compared with the galaxy spectra in our sample. After all spectra were normalized to the continuum, this program slides the template spectrum across the measured galaxy spectrum and calculates the difference between the two spectra at each point. The shift corresponding to the smallest difference between the spectra is used to calculate the redshift of the galaxy in question. This method, unlike measuring the absorption features by hand, does not depend on determining the center of blended lines.

There were a small number of galaxies in each KISSR GP field whose spectra contained identifiable emission lines but were also well measured using FXCOR for the absorption features. We used these as test cases to make sure that FXCOR was working properly with our template spectra. For these galaxies, the FXCOR redshift measurements agreed with the WRALF redshift measurements well in all cases. The FXCOR and WRALF redshift comparison will be presented in a separate paper.

Full details of our redshift survey, including the publication of all new spectroscopic redshifts and their comparison with corresponding SDSS photometric redshifts, will be presented in a forthcoming paper (S. W. Brunker et al. 2022, in preparation).

2.3. Depth and Completeness of the Redshift Survey

In order to analyze the density of galaxies around the GPs and conclude something about their environments, we need to quantify the depth and completeness of our survey. For all but two of our GP fields, we selected targets down to $g = 21$. For the remaining two fields, we extended this magnitude limit by 0.3 and 0.2 magnitudes in order to include a sufficient number

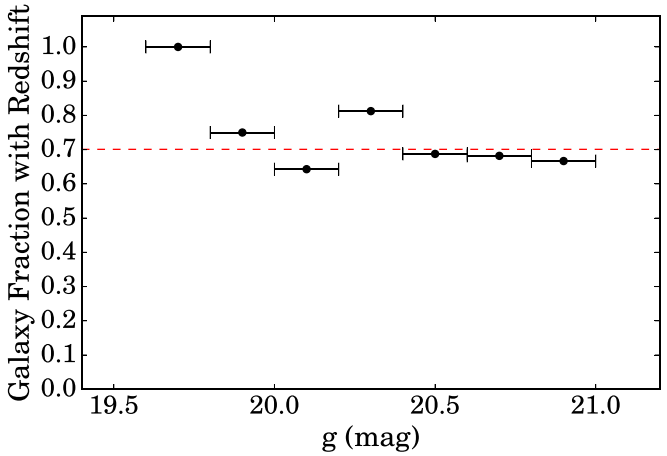

Figure 3. The redshift survey completeness for the KISSR 1791 field. The completeness fraction is plotted as a function of the g magnitude. In each magnitude bin, the galaxy fraction is the total number of galaxies with a measured redshift (our survey measurements and existing SDSS spectroscopic redshifts) divided by the total number of SDSS galaxies in the field that fit the selection criteria (shown in Figure 2). We measured 75 galaxy redshifts for the KISSR 1791 field, and there were 7 galaxies for which we were unable to measure a redshift. Additionally, we obtained SDSS redshifts for 7 galaxies in the field, which had been previously observed and thus were not included as possible observing targets. The red dashed line indicates the overall completeness for the field. There is essentially no magnitude dependence on the completeness.

of target galaxies. When selecting targets we focused more on observing as many galaxies close to the GP rather than ranking them by their brightness.

We calculate the completeness of our survey for each KISSR GP field as a function of the g magnitude. For each g magnitude bin, we counted the number of galaxies in our survey that had a measured redshift and added the number of galaxies for which the SDSS already had a measured spectroscopic redshift in the field. We then divided that number by the total number of SDSS galaxies in the field that fit our selection criteria (e.g., photometric redshift cuts and g-magnitude cut). We show this fraction as a function of the g magnitude for KISSR 1791 in Figure 3. Most of the KISSR GP fields show a relatively flat completeness curve out to the magnitude limit of $g = 21$. Therefore, our redshift survey completeness is not very dependent on the apparent magnitude.

Table 2 summarizes the results of our redshift survey for each of the GP fields. The g-magnitude limit, total number of possible observing targets, number of galaxies observed in our redshift survey, and success rate of our redshift measurements are listed in columns 2–5. On average, 91.5% of our spectroscopic targets yielded a redshift measurement. The total number of galaxies with a measured redshift (combined number from our observations plus existing SDSS spectroscopic redshift values) and the completeness percentage are presented for each GP field in columns 6–7. The average completeness percentage across our 13 survey fields is 57%. We calculated the absolute magnitude limit we would be able to observe at the distance of each GP and present that in column 8. The last three columns in Table 2 refer to results from the environmental analysis that is presented in the following two sections. Column 9 is the distance to the galaxy closest to the GP (nearest-neighbor distance). We present the 1D cylindrical density at the distance of the GP in column 10. Based on the results of the environmental analysis for the 13 KISSR GPs, we grouped galaxies into five environment groups, and those are presented in column 11.

To summarize the work we completed in undertaking this environment survey: we observed and reduced spectra and measured redshifts for 1312 galaxies distributed between 13 KISSR GP fields.

3. GP Environment Density Analysis

After completing our redshift survey for our KISSR GP targets, the next step is to visualize and analyze the environments in which the GPs are found. We have constructed redshift position diagrams (pencil-beam diagrams) for all of the objects in our survey. This allows us to visualize the redshift distribution of galaxies in each GP field. Figure 4 shows a detailed version of the pencil-beam plots for KISSR 847. The left-hand side shows the R.A. projection and the right-hand side shows the Decl. projection. The central red point is the KISSR GP, the black points are galaxies whose distances were measured in this survey, and the gray points are galaxies which already had spectroscopic redshifts from the SDSS. The top plots show a version of the pencil beam that extends 500 Mpc on either side of the KISSR GP galaxy. The concentric circles designate increasing distances from the central GP. The middle and bottom plots are zoomed-in panels of the pencil beam that extend 200 and 60 Mpc on either side of the central GP, respectively. The complete set of pencil-beam diagrams is presented in S. W. Brunker et al. (2022, in preparation).

The upper two plots showing the extended version of the pencil beam allow us to see the larger structures of filaments and voids even though we are only mapping a narrow slice of space. By zooming in, the bottom plots show more of the immediate environments of the KISSR GPs, which is crucial for understanding the connection between the star formation in the GPs and their environments. Of course we can characterize the KISSR GP environments by eye, but we also decided to analyze our pencil beams using three distinct density estimators for a more quantitative analysis. The three density estimators we chose to use are: (1) a cylindrical density analysis along the pencil beam; (2) a spherical shell density analysis centered on the KISSR GP; and (3) a nearest-neighbor distance calculation for the GP and the other galaxies in the survey. These methodologies are sampling the environment in a variety of spatial scales. We selected these methods because they were most suitable for the geometry of our survey volume. Each of these three density estimation methods has its limitations, and we attempt to gain a more complete picture by using more than just one density estimator. By comparing all three of these density estimators with the pencil-beam plots for each KISSR GP field, we gain a better understanding of what the immediate environments for these GP galaxies look like.

3.1. Cylindrical Density Analysis

To create a density profile for the KISSR GP fields, we moved a fixed-length cylinder along the pencil beam and counted the number of galaxies within it to determine the density within the cylinder. We chose the length of the cylinder to be 15 Mpc, which is close to the average radius of the pencil beams for the KISSR GPs. We moved the cylinder along the pencil beam in steps half the length of the cylinder, so there was some overlap in the volume in which we calculated the density. Because the radius of the pencil beam increases with the distance, we chose the radius for our cylinder to be the radius of the pencil beam at the higher-distance end of the

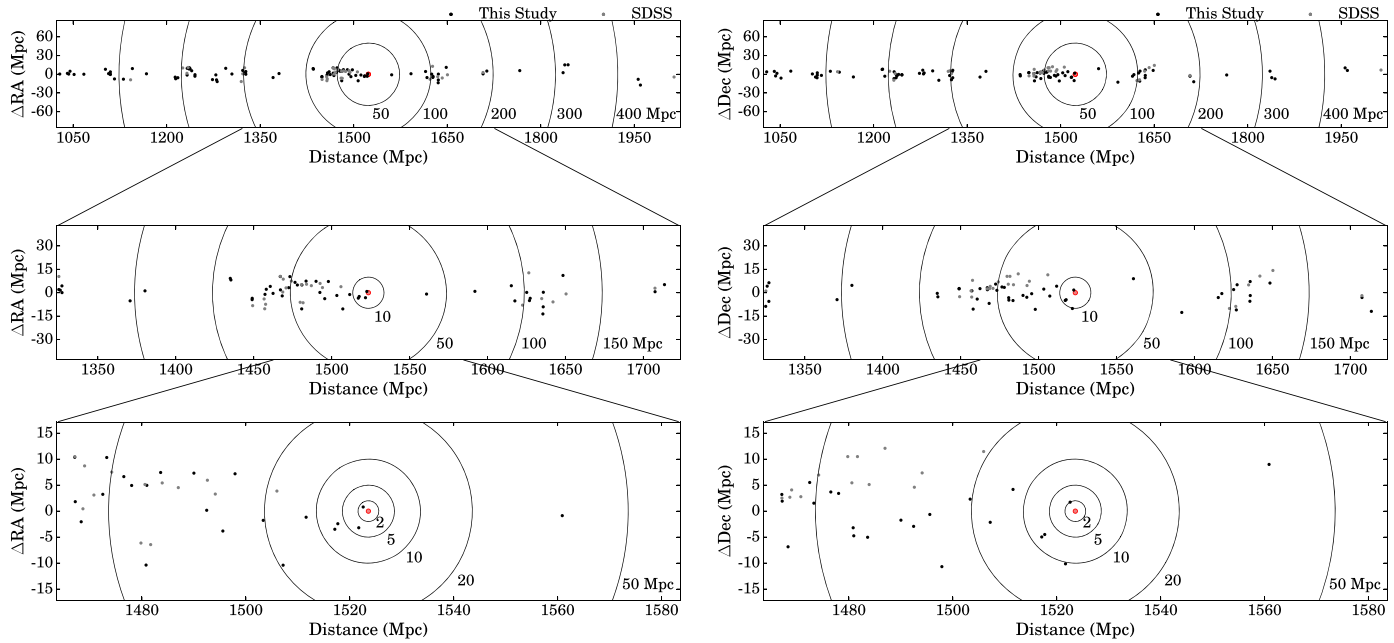

Figure 4. Redshift-position diagrams (pencil-beam diagrams) for the KISSR 847 field. The left-hand side shows the R.A. projection, and the right-hand side shows the Decl. projection. The top plots show the pencil beam extended to 500 Mpc on either side of KISSR 847, which is indicated by the central red point. The black points are the galaxies whose redshifts were measured in this survey, and the gray points are galaxies with existing SDSS spectroscopic redshifts. The concentric circles indicate increasing distances from the central GP. The middle and bottom plots are zoomed-in panels of the pencil beam that extend to 200 and 60 Mpc on either side of KISSR 847, respectively.

Table 2
KISSR Green Peas—Environment Survey

KISSR	g mag. limit	# Gal. in Photo-z Range	# Gal. Observed	Obs. Success Rate (%)	# Gal. with Measured z	Completeness (%)	M_g Limit	NN Distance (Mpc)	Cylindrical Density at GP (Mpc^{-3})	Environment Group
(1)	(2)	(3)	(4)	(5)	(6)	(7)	(8)	(9)	(10)	(11)
225	21.0	208	109	87	113	54	−19.93	53.88	5.03×10^{-5}	EI
560	21.0	230	117	79	100	43	−19.93	3.58	1.48×10^{-3}	LD
847	21.0	206	104	96	130	63	−19.92	2.11	1.36×10^{-3}	ID
1038	21.3	129	90	97	101	78	−19.92	8.69	6.23×10^{-4}	EI
1290	21.0	297	130	95	137	46	−19.58	1.07	4.29×10^{-3}	ID
1508	21.0	412	128	83	129	31	−19.50	9.22	4.94×10^{-4}	EI
1516	21.0	281	116	96	134	48	−19.74	7.00	1.22×10^{-3}	EI
1759	21.2	161	117	87	120	75	−20.00	3.12	1.27×10^{-3}	ID
1791	21.0	117	82	91	82	70	−19.94	8.00	6.02×10^{-4}	EI
1825	21.0	258	136	100	149	58	−19.76	2.78	1.98×10^{-3}	ID
1953	21.0	137	82	91	89	65	−19.99	13.41	2.09×10^{-4}	EI
2005	21.0	317	115	94	139	44	−19.60	3.02	2.00×10^{-3}	ID
2042	21.0	170	96	93	107	63	−19.92	4.43	6.78×10^{-4}	EI

cylinder. Hence, the volume of the cylinder increases slightly as we move it along the pencil beam. We created the density profile of the KISSR GP pencil beams to a distance of 100 Mpc on either side of the GP. We visualized the results of this density estimation analysis by plotting the density versus the distance, marking the distance of the KISSR GP using a dashed red line. An example result for this analysis (using the same KISSR GP field as in Figure 4) is shown in Figure 5 in the second plot from the top. It appears that KISSR 847 is located on the edge of a higher-density region in the pencil beam.

The cylindrical density was also calculated with the cylinder centered on the KISSR GP, and the results are presented in column 8 of Table 2. We utilize this value as the best estimate of the global density in the vicinity of each GP. In the case of KISSR 225, there are no galaxies located within the default cylinder, so we extended the length to 110 Mpc in order to calculate a nonzero density. Two other GPs had the same problem, though the cylinder did not need to be extended much compared to KISSR 225. For KISSR 1508, we extended the cylinder to a length of 17 Mpc, and for KISSR 1953, we extended the cylinder length to 22 Mpc.

We applied two corrections to the measured density values for each GP. The first is a correction for the incompleteness of our redshift survey. As shown in Table 2, not all galaxies in our survey fields with the correct photoz range have measured redshifts. We multiplied the measured density values by the inverse of the completeness given in column 5 of Table 2 to account for the unobserved galaxies. This correction assumes

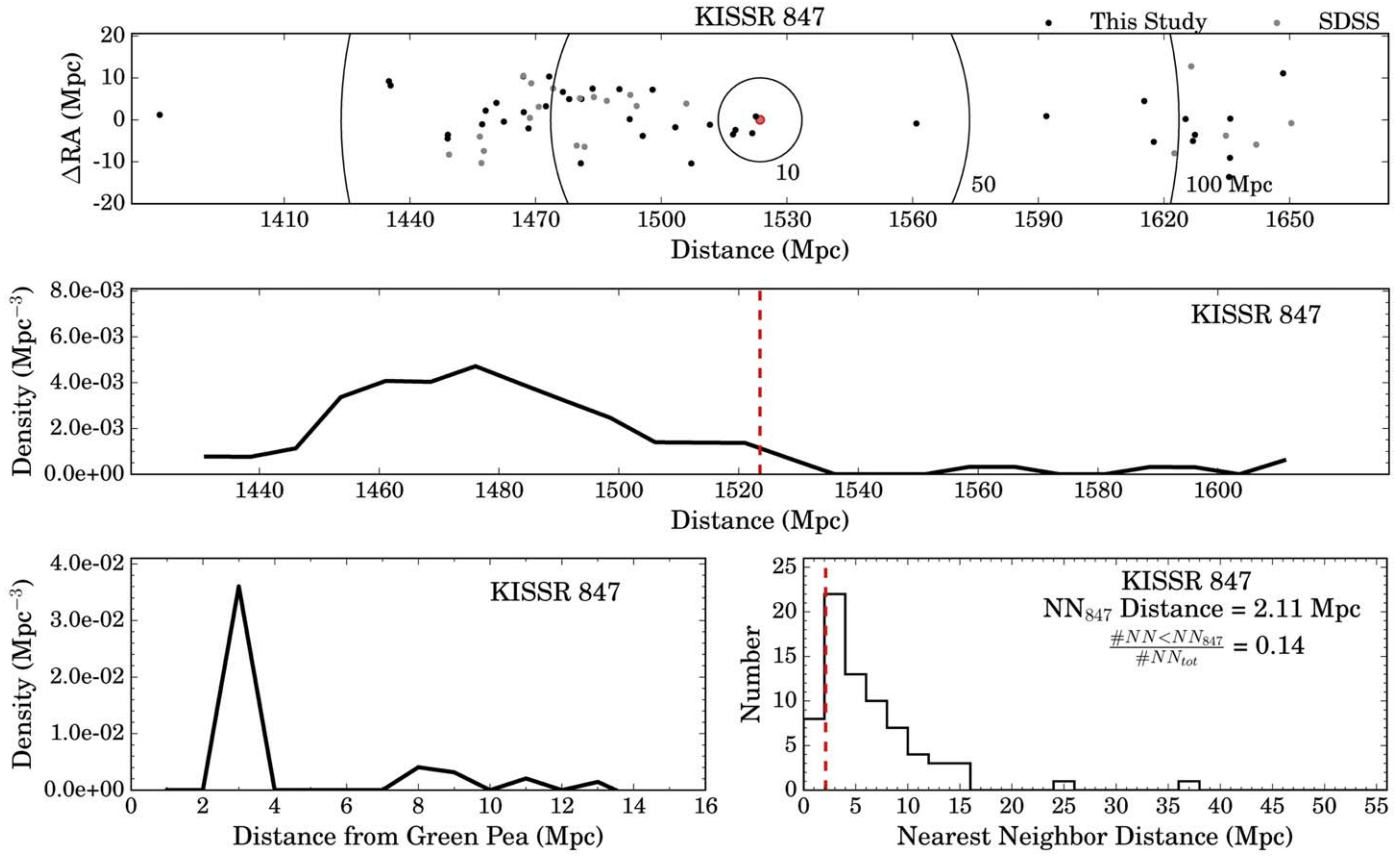

Figure 5. Combined density analysis plots for KISSR 847. Top: A pencil-beam diagram showing the R.A. projection for KISSR 847 that extends to 150 Mpc on either side of the GP. This provides a visualization of the data for comparison with the density plots. Middle: Cylindrical density profile for the KISSR 847 field. To calculate the density along the pencil beam, we moved a fixed-length cylinder along the pencil beam and counted the number of galaxies within the cylinder at each point to calculate the density. The calculated densities have been corrected for the survey incompleteness and the difference in depth for each GP field. Bottom Left: A visualization of the spherical shell density analysis for KISSR 847. We calculated the density in a series of spherical shells going outward from KISSR 847 each with a constant width of 1 Mpc. We did not go past the radius of the pencil beam at the distance of KISSR 847. These density values have been corrected in the same way as the cylindrical density profile. Bottom Right: Nearest-neighbor analysis for KISSR 847. We calculated the nearest-neighbor distance for KISSR 847, and we did the same for all the other galaxies in the pencil beam within ±200 Mpc of the GP. The nearest-neighbor distance for KISSR 847 is printed in the top right of the plot and shown as a red dashed vertical line. The histogram shows the distribution of nearest-neighbor distances for the galaxies in the survey. The legend also includes the quantity $\frac{\#\,\mathrm{NN} < \mathrm{NN_{KR}}}{\#\,\mathrm{NN_{tot}}}$. This quantity parameterizes the fraction of galaxies in the field with nearest-neighbor distances smaller than the GP. This tells us how the nearest-neighbor distance for KISSR 847 compares to other galaxies within 200 Mpc. This density analysis differs from the others shown because the nearest neighbor looks at only the closest galaxy to the GP, not the full environment around the GP.

that the redshift distribution of the unobserved galaxies will be similar to that of the observed ones. The second correction accounts for the fact that the depth to which our redshift survey samples is different for each GP. Because our survey is magnitude-limited, at larger distances the measured densities will decrease because of the decreased depth. The luminosity-function normalization method (Postman & Geller 1984) corrects the densities for decreased sampling at higher redshifts. We used this method to correct our densities with the luminosity function parameters derived by Blanton et al. (2003) for SDSS galaxies ($M_g^* = -20.1$ and $\alpha = -0.89$). These corrections allow us to put all of our survey fields onto the same density scale, for more effective intercomparisons.

3.2. Spherical Shell Density Analysis

To better probe the densities in the immediate area around the KISSR GP, we use a spherical shell density estimation analysis. While this type of analysis is commonly used in extragalactic environment studies, it does not lend itself as well to the current project. First, the geometry of our survey volume is inherently cylindrical rather than spherical. Second, this type of measurement makes use of only a small fraction of our measured redshifts. Nonetheless, we feel it is a useful statistic of the density environment close to our GPs, particularly when used in conjunction with our two other measures of the environment.

We calculated the density of galaxies in a series of spherical shells going outward from the central KISSR GP. We kept the width of the spherical shells as a constant 1 Mpc, and we did not go past the radius of the pencil beam at the distance of the KISSR GP. We again applied the correction for the incompleteness of our redshift survey and the correction accounting for the differing depths of our redshift survey samples for each GP field. The result of this analysis for KISSR 847 is shown in the bottom left plot in Figure 5. Similar to the 1D density profile result, we again plot the density versus the distance, but in this case the distance is from the central KISSR GP, not the distance from us. For KISSR 847, we see the first nonzero density between 2 and 4 Mpc, not close enough to be actively interacting with KISSR 847.

3.3. Nearest Neighbor Analysis

The third method we used to quantitatively analyze the KISSR GP environments was to look at the nearest-neighbor

distance for the GP compared to the nearest-neighbor distance for the other galaxies within ±200 Mpc of the KISSR GP in the pencil-beam survey. The process for this analysis is fairly simple. We calculated the distance from the GP to all the other galaxies within 200 Mpc, and the nearest-neighbor distance is the distance to the galaxy closest to the GP. We repeated this process for each of the other galaxies within 200 Mpc of the GP. The results of this comparison are shown in the bottom right plot in Figure 5. We present a histogram showing the number of galaxies with a given nearest-neighbor distance. The nearest-neighbor distance for KISSR 847 is printed in the upper right hand corner of the plot, 2.11 Mpc, and is also represented as a red dashed vertical line. We also derive a measurement of the isolation of the GP where we measure the percentage of galaxies with nearest-neighbor distances less than the nearest-neighbor distance for the GP. The equation we use, which is also presented in the nearest-neighbor plot, is given as

$$\frac{\#NN < \mathrm{NN_{KR}}}{\#\mathrm{NN_{tot}}}.$$

The numerator ($\#\mathrm{NN} < \mathrm{NN_{KR}}$) is the number of galaxies with nearest-neighbor distances less than the nearest-neighbor distance of the KISSR GP (represented by $\mathrm{NN_{KR}}$). We divide this number by the total number of galaxies for which we measured nearest-neighbor distances. This fraction tells us how the nearest-neighbor distance of the KISSR GP compares with the nearest-neighbor distances for other galaxies within 200 Mpc of the GP. This measurement tells us more about the typical large-scale structure along the pencil beam in each field than the immediate environment around the GP. For KR 847, only 14% of galaxies have nearest-neighbor distances smaller than KISSR 847.

3.4. Combining the Density Estimator Analyses

By taking into account the results from these three density estimators along with a visual evaluation of the galaxy distribution within the pencil beams for each KISSR GP field, we gain a better idea of what kind of environment the KISSR GPs are found in. We use the cylindrical density estimator to look at the density of galaxies around the GP compared with the densities measured along the pencil beam. We use the spherical density estimator and the nearest-neighbor analysis to gain a better understanding of the immediate environments around the GPs. We combine these three density estimators and compare them with the qualitative visual representation of the environments that we see in the pencil-beam diagrams to reach our final environment determination. For example, KISSR 847, shown in Figure 5, is found on the edge between a fairly high-density galaxy structure and a void region. KISSR 847's nearest neighbor is 2.11 Mpc away, which is not that large of a separation compared with the nearest-neighbor distances of other galaxies in the pencil beam. By looking at the density at increasing radii from KISSR 847, we can conclude that the GP does not live in an overly dense environment like a cluster or large group of galaxies. This is all seen qualitatively in the pencil-beam diagram at the top of Figure 5, but by looking at these quantitative density estimations, we can directly compare the environments of the 13 KISSR GP fields presented in this study. The three methodologies allow us to sample different spatial scales and gain a more holistic view of the GP environments.

The density plots for all 13 KISSR GPs are presented in the following section.

4. Discussion: KISS GP Environments

4.1. Results of the GP Density Analysis

By evaluating the density estimators for the individual GP environments, we are better able to study the nature of each GP in our sample. By looking at the results of the environment analysis more broadly, it also allows us to understand the GPs as a class of galaxies. We want to understand the range of environments that GPs are found in and how these environments relate to specific GP properties, such as their their star formation rates.

The combined density estimator plots for all 13 KISSR GP galaxies are presented in Figures 5−17. In each figure, the top plot is a pencil-beam plot out to 150 Mpc from the GP using the R.A. projection. The middle plot is the 1D density profile for that GP field. The bottom left plot is the spherical shell analysis, and the bottom right plot is the nearest-neighbor analysis.

We will present a brief description of each field before we discuss the aggregate results of our environmental analysis of the KISS GPs. As part of our analysis of each field, we will categorize the environment around each GP into one of the following five groups: (1) very low density/extremely isolated (EI); (2) low-density environment, tending toward isolation (LD); (3) intermediate-density environment, as in a sparse filament (ID); (4) higher density, as in a populous filament (HD); and (5) a cluster environment (CL). By assigning the GPs to an environment group, we are able to take into account all of the information available for each object, rather than relying on a single quantity to parameterize its environment.

KISSR 225 KR 225 is clearly located in a void, as seen in Figure 6. There are no galaxies within 50 Mpc of the GP, so it is classified as extremely isolated (EI).

KISSR 560 The immediate environment around KR 560 includes a few galaxies within 10 Mpc, though the closest galaxy to KR 560 is 3.58 Mpc away, as shown in Figure 7. There is a large number of galaxies a little more than 10 Mpc away, and KR 560 is found on the edge between a more dense region and a void. We classify it as low density (LD) based in large part due to the nearest-neighbor distance.

KISSR 847 There are four galaxies within 10 Mpc of KR 847, and the closest one is 2.11 Mpc away. KR 847 is clearly located on the edge of a more dense collection of galaxies, but there are no galaxies within ∼40 Mpc at larger distances, as seen in Figure 5. KR 847 has a denser immediate environment than KR 560, so we classify it as intermediate density (ID).

KISSR 1038 As seen in Figure 8, the closest galaxy to KR 1038 is 8.69 Mpc away, and it is the only galaxy within 10 Mpc of the GP. There are several galaxies between 10 and 20 Mpc away from KR 1038, but it is clear that the GP is found in a very-low-density environment (EI).

KISSR 1290 There are a dozen galaxies within 10 Mpc of KR 1290, the closest being 1.07 Mpc away as seen in Figure 9. While this looks like a dense environment compared to the previous GP fields, it is not dense when compared with large galaxy groups or clusters. The Milky Way and Andromeda are closer to each other than KR 1290 is to its nearest neighbor. We consider it to be in an intermediate-density environment (ID).

KISSR 1508 KR 1508, shown in Figure 10, is another GP in an environment that is essentially a void. The closest galaxy to KR 1508 is 9.22 Mpc away, and there are only two other galaxies within 50 Mpc of the GP. Our survey does detect two

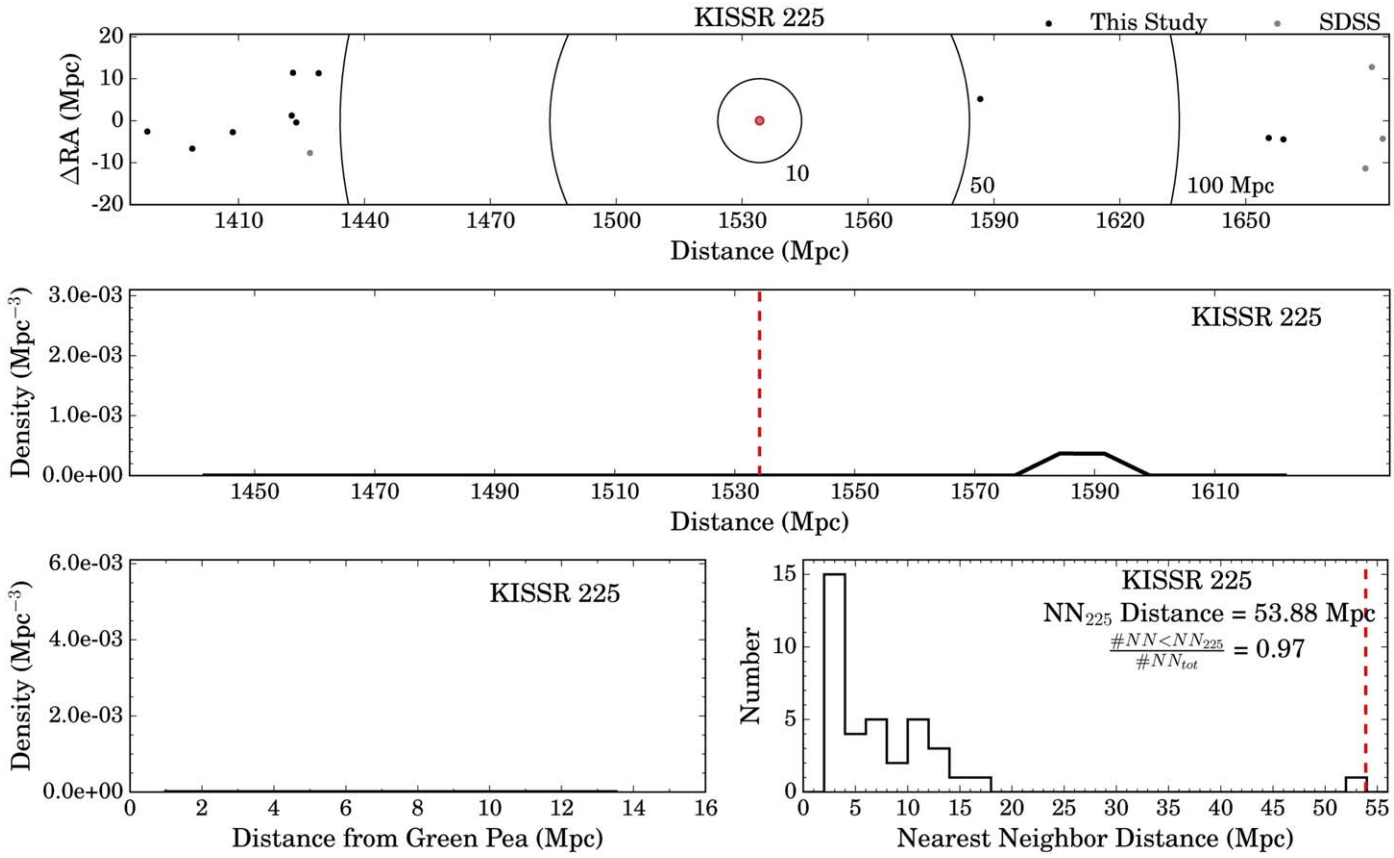

Figure 6. Combined density analysis plots for KISSR 225. The layout and meaning of the various plots are described in detail in the caption of Figure 5.

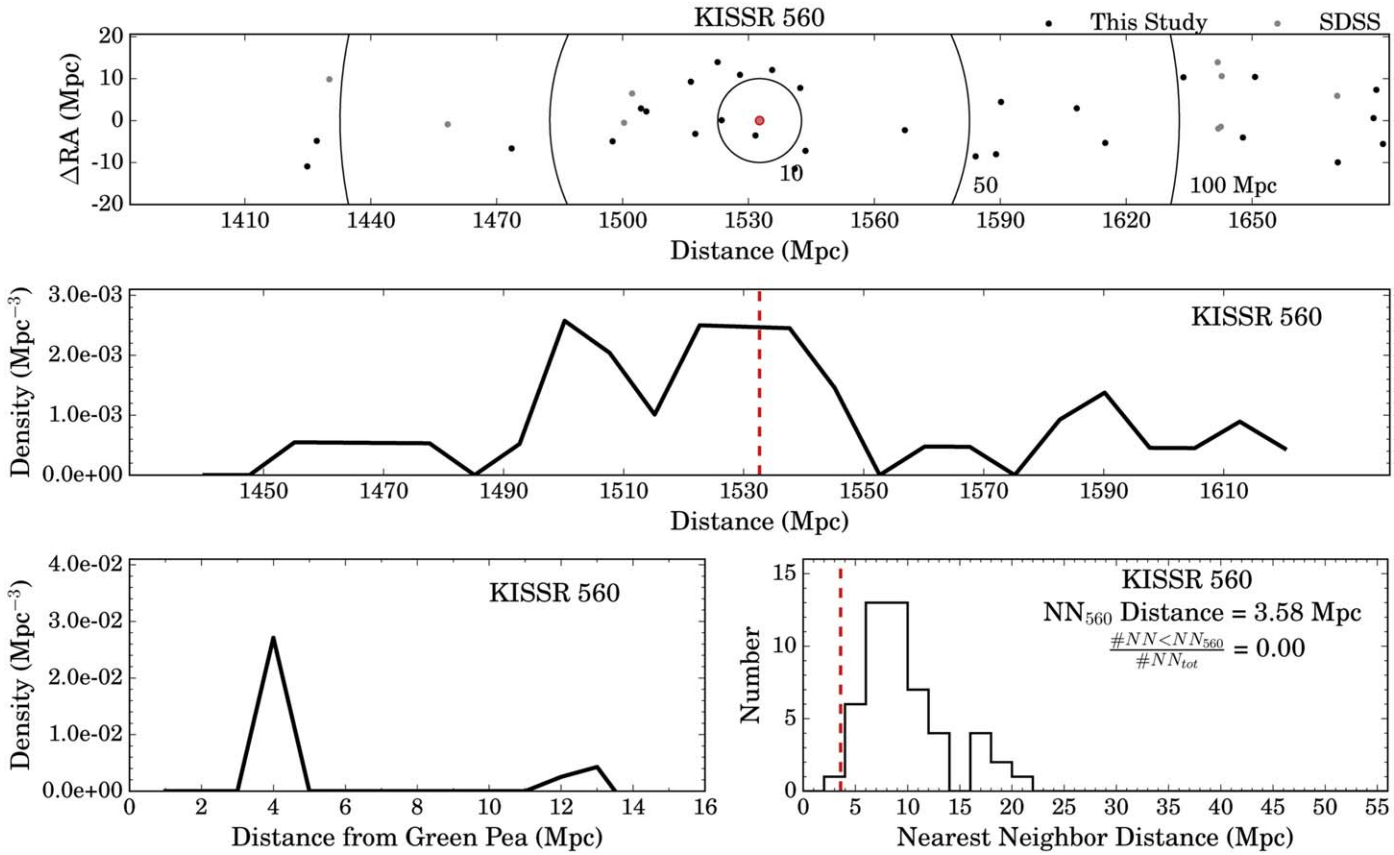

Figure 7. Combined density analysis plots for KISSR 560. The layout and meaning of the various plots are described in detail in the caption of Figure 5.

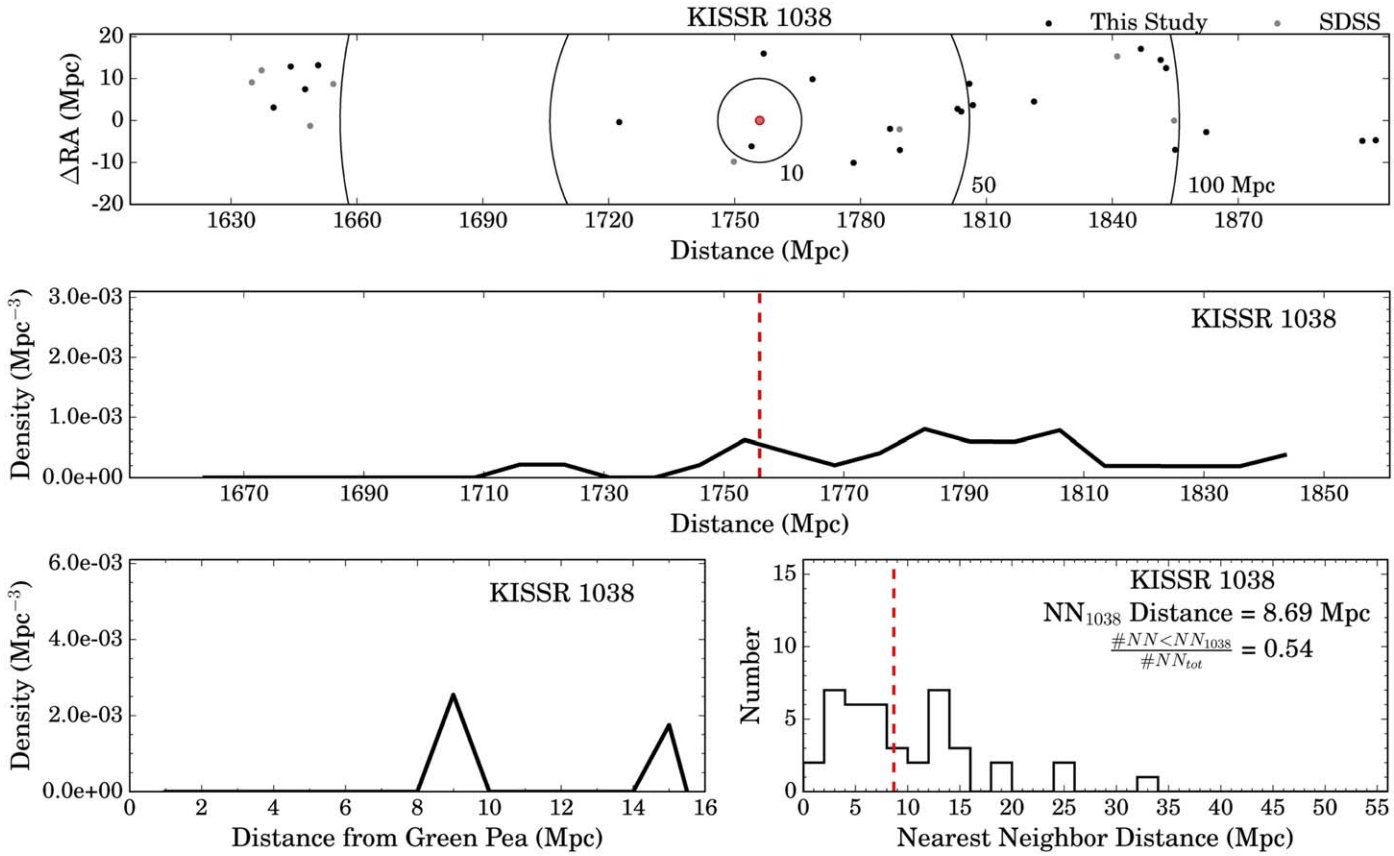

Figure 8. Combined density analysis plots for KISSR 1038. The layout and meaning of the various plots are described in detail in the caption of Figure 5.

higher-density structures both in front of and behind KR 1508. KR 1508 is classified as extremely isolated (EI).

KISSR 1516 KR 1516 is similar to KR 1038. There are two galaxies within 10 Mpc of KR 1516, and the closest is 7 Mpc away, as shown in Figure 11. There are a couple of galaxies within 20 Mpc of the GP, but otherwise it resides in a very-low-density environment (EI).

KISSR 1759 As seen in Figure 12, there are five galaxies within 10 Mpc of KR 1759. The closest one is 3.12 Mpc away from the GP. There are a handful of galaxies further away within 20 Mpc of KR 1759. The immediate environment around the GP is similar to KR 847, and the local density is high enough to warrant an intermediate density (ID) classification.

KISSR 1791 KR 1791 is another GP that is found in essentially a void, as shown in Figure 13. The closest galaxy to the GP is 8 Mpc away, and there are two other galaxies around 10 Mpc away from KR 1791. There are not that many other galaxies within 50 Mpc of the GP, so we classify it as extremely isolated (EI).

KISSR 1825 The environment around KR 1825, shown in Figure 14, is similar to those around KR 847 and KR 1759. There are five galaxies within 10 Mpc of the GP, and the closest is 2.78 Mpc away. KR 1825 also appears to be on the edge between a moderately high-density region and a foreground void. We classify it as an intermediate density environment (ID).

KISSR 1953 KR 1953 is located in a void, as shown in Figure 15. The closest galaxies to the GP is 13.41 Mpc away, and there are just a handful of galaxies within 50 Mpc of KR 1953. It clearly lives in a very-low-density environment (EI).

KISSR 2005 Shown in Figure 16 are four galaxies within 10 Mpc of KR 2005, and the closest one is 3.02 Mpc away from the GP. There are a handful of galaxies within 20 Mpc of KR 2005, and while the immediate environment could not be called dense, it is denser than many of the other GP environments in our sample. We classify it as an intermediate-density environment (ID).

KISSR 2042 The closest galaxy to KR 2042 is 4.43 Mpc away, but that is the only galaxy within 10 Mpc of the GP, as seen in Figure 17. There are only a handful of galaxies within 50 Mpc of KR 2042, so it is clear that this GP is found in an environment that is essentially a void (EI).

4.2. Characterizing the KISSR GP Environments

As explained in the previous subsection, we analyzed the results from the different density estimators to quantify, roughly, what kind of environment each GP lives in. We have chosen to group the GPs into one of five categories based on our analysis: (1) extremely low-density environments; (2) low-density environments but tending toward isolation; (3) intermediate-density environments, as in a sparse filament; (4) higher-density environments, as in a populous filament; and (5) a cluster environment. These classifications are simple, but they are the starting point for a deeper understanding of what role a GP's environment plays in its formation and evolution. In addition to grouping the GPs into specific categories, we also looked at the larger general environmental trends apparent in our survey data, and we will discuss this at the end of the section.

We stress that there is no one single density parameter that can be used to assign a given GP into one of the environmental categories listed above. Rather, as mentioned earlier, we look at all of the available information before assigning a galaxy into

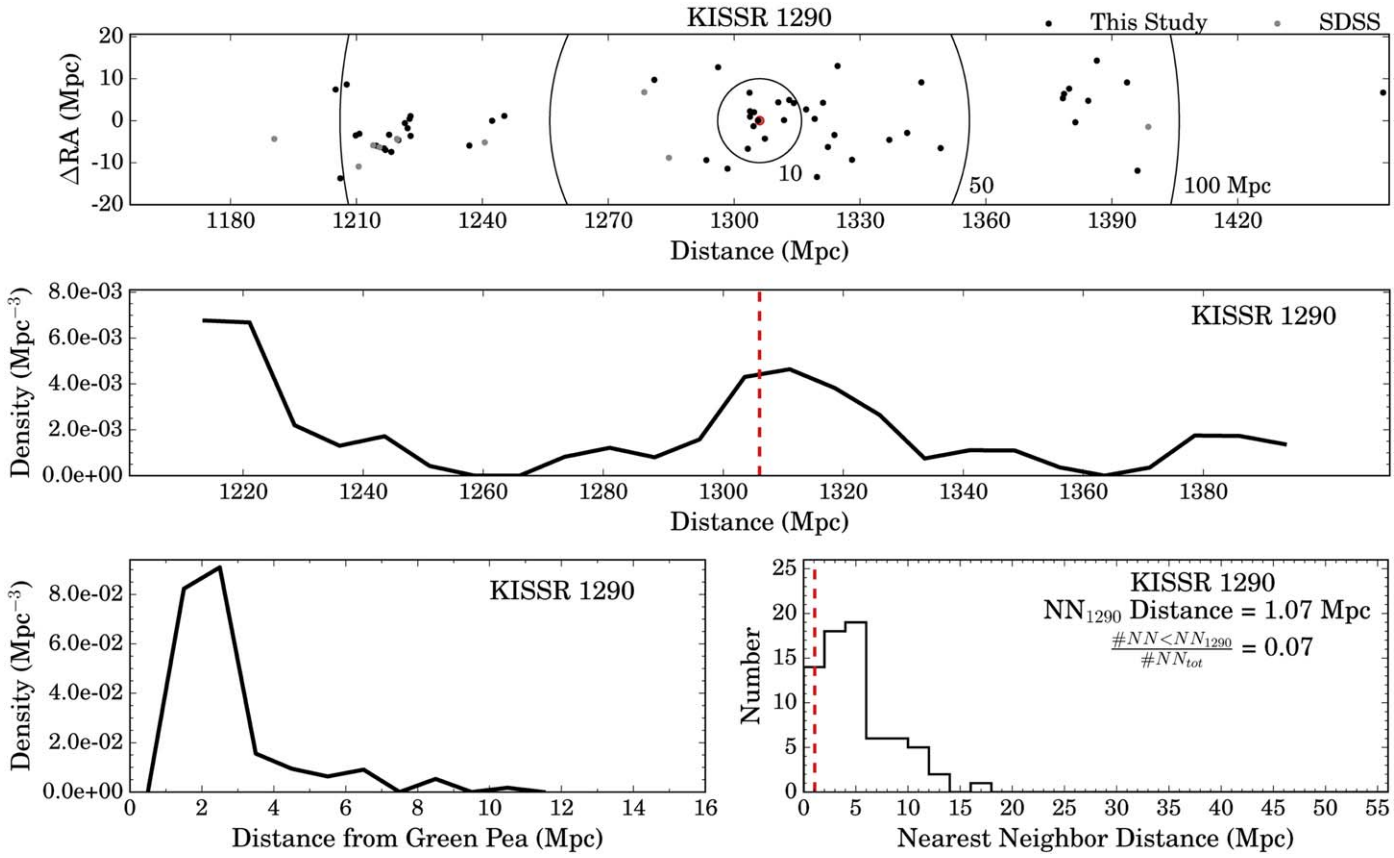

Figure 9. Combined density analysis plots for KISSR 1290. The layout and meaning of the various plots are described in detail in the caption of Figure 5.

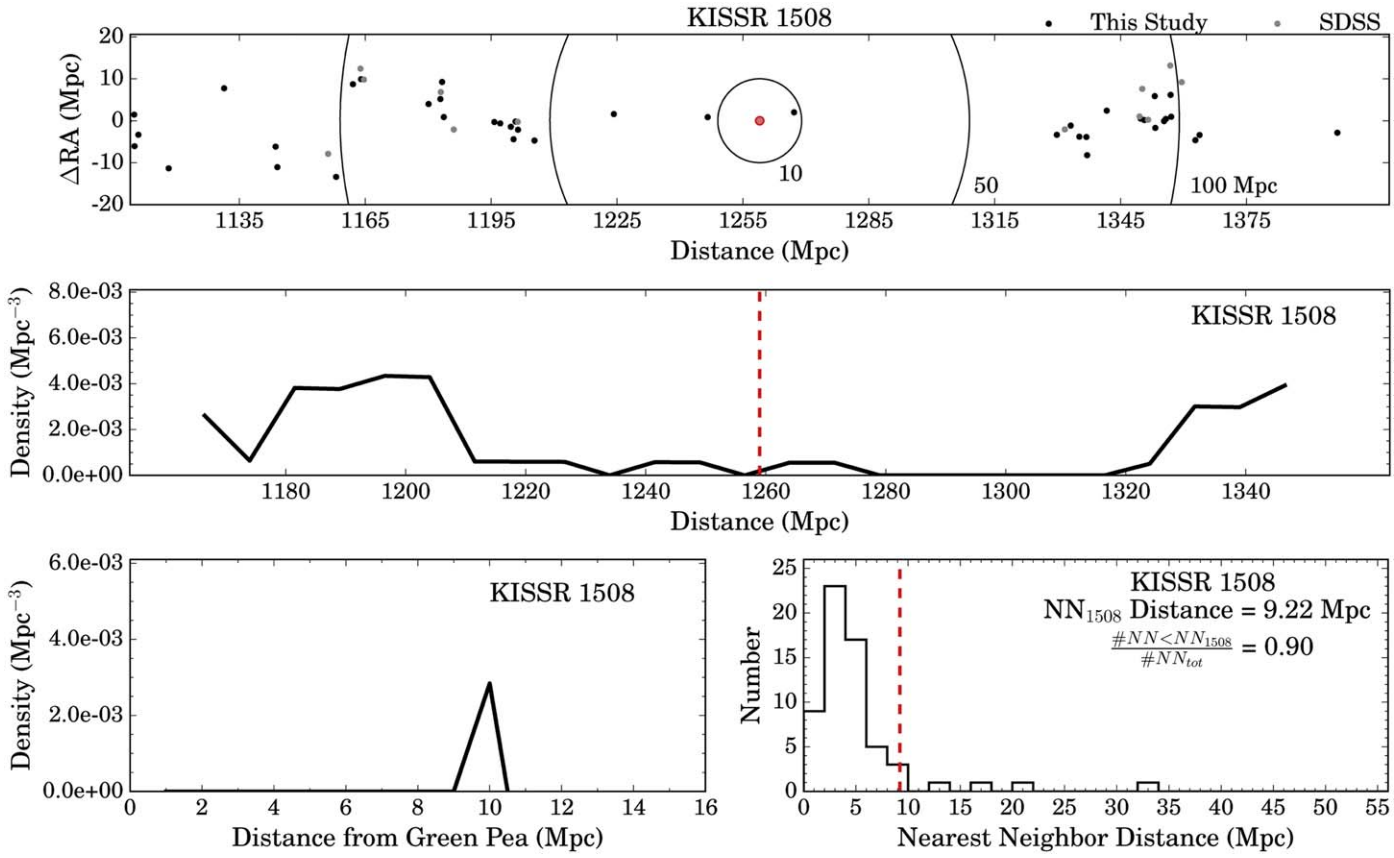

Figure 10. Combined density analysis plots for KISSR 1508. The layout and meaning of the various plots are described in detail in the caption of Figure 5.

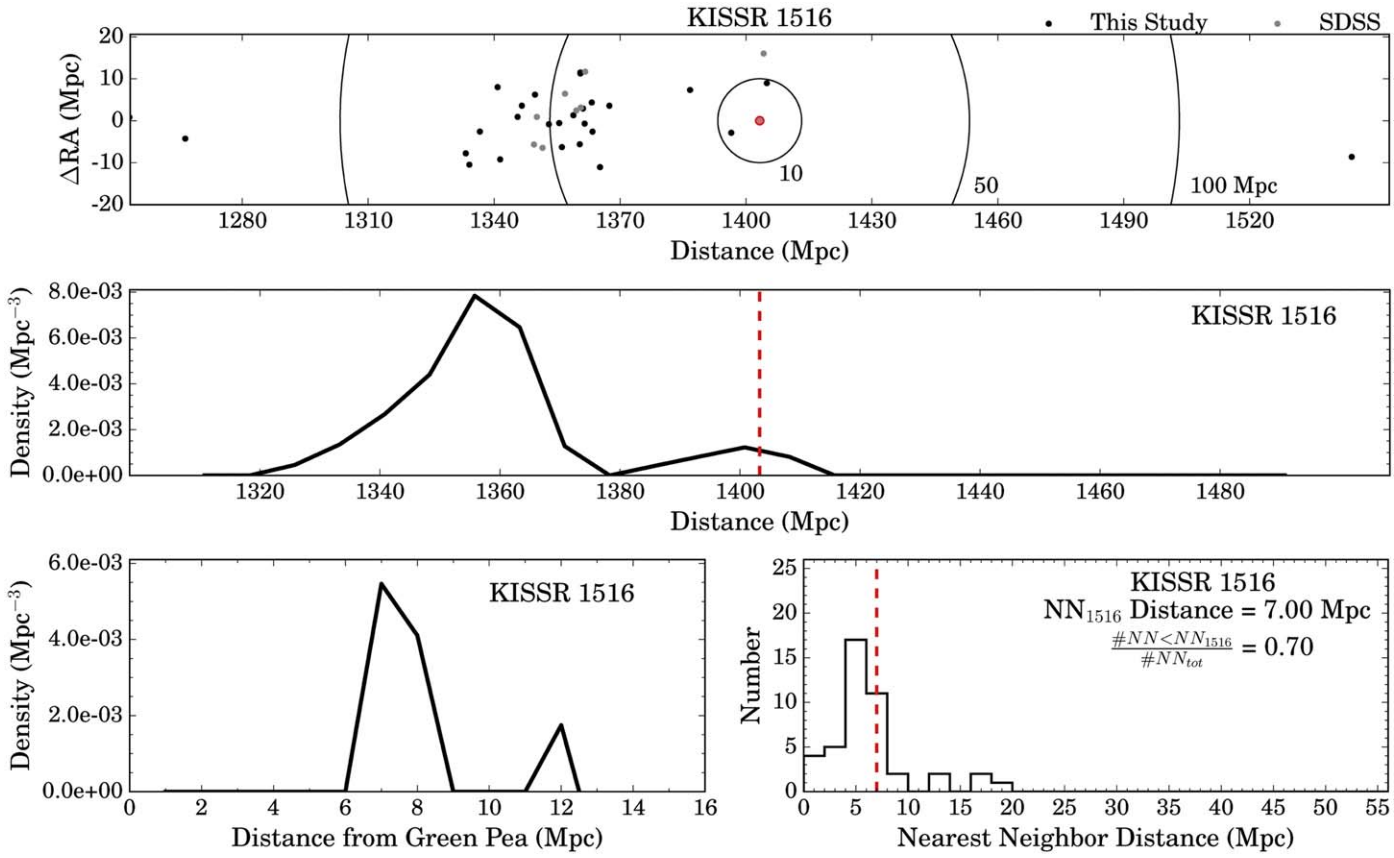

Figure 11. Combined density analysis plots for KISSR 1516. The layout and meaning of the various plots are described in detail in the caption of Figure 5.

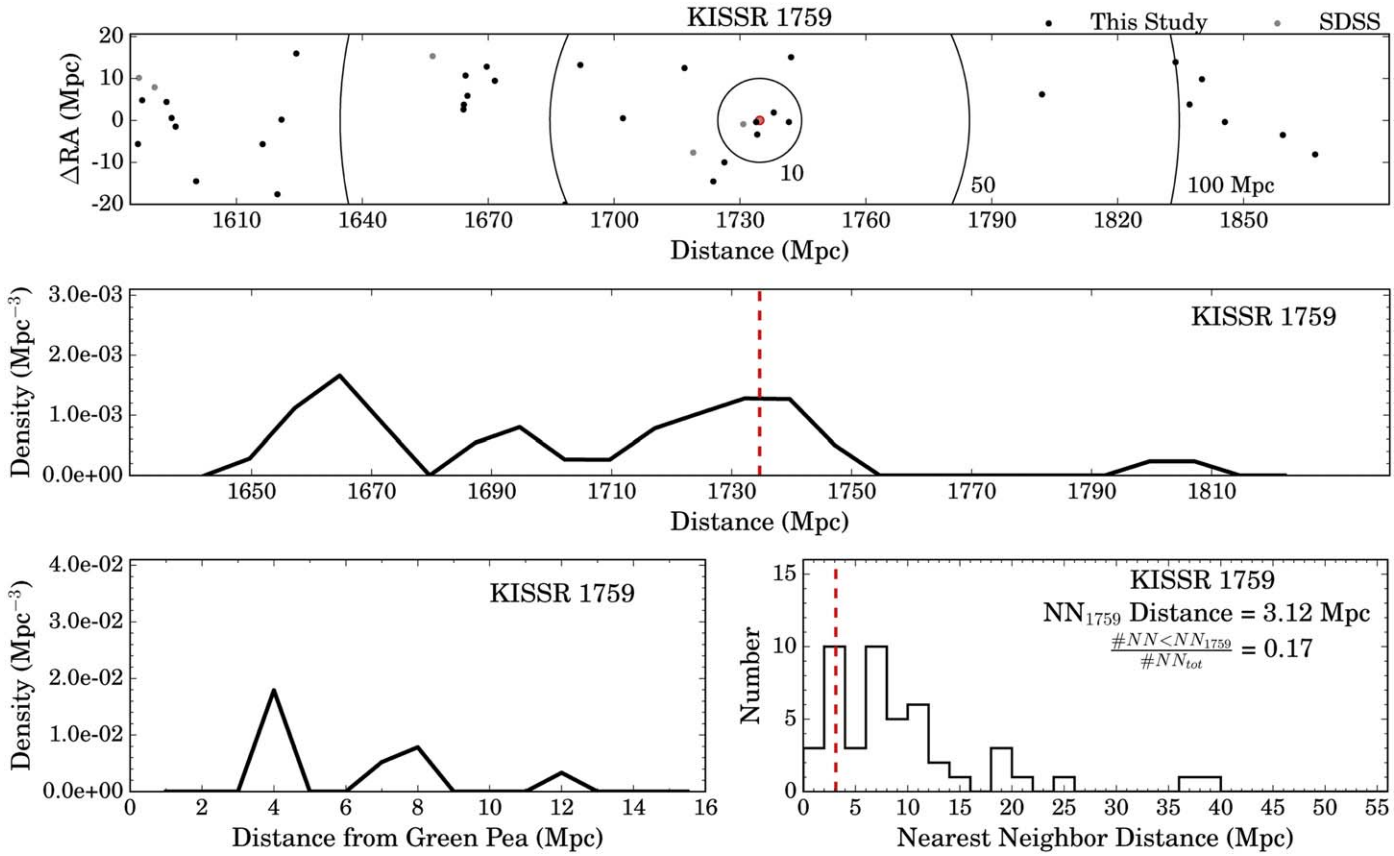

Figure 12. Combined density analysis plots for KISSR 1759. The layout and meaning of the various plots are described in detail in the caption of Figure 5.

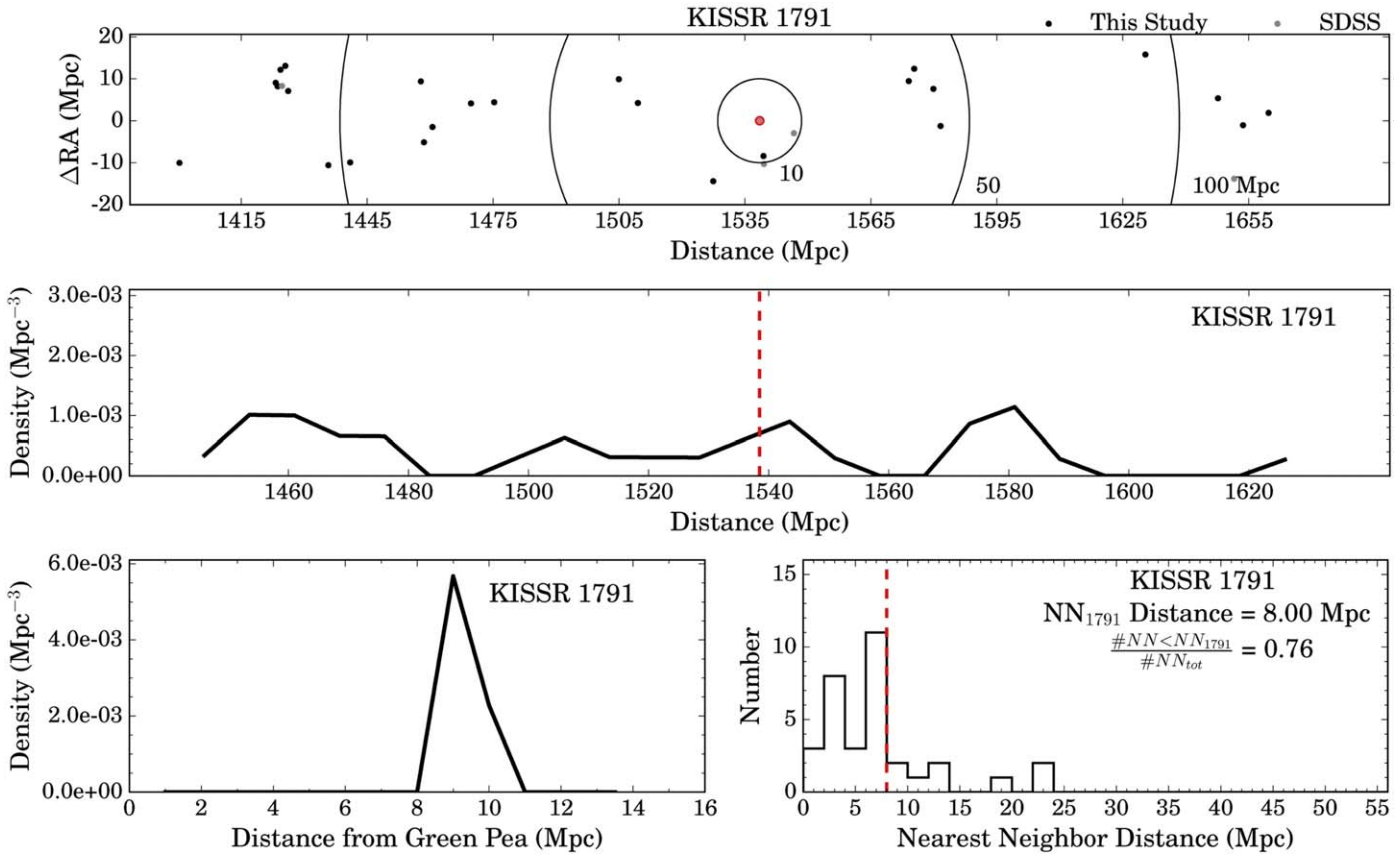

Figure 13. Combined density analysis plots for KISSR 1791. The layout and meaning of the various plots are described in detail in the caption of Figure 5.

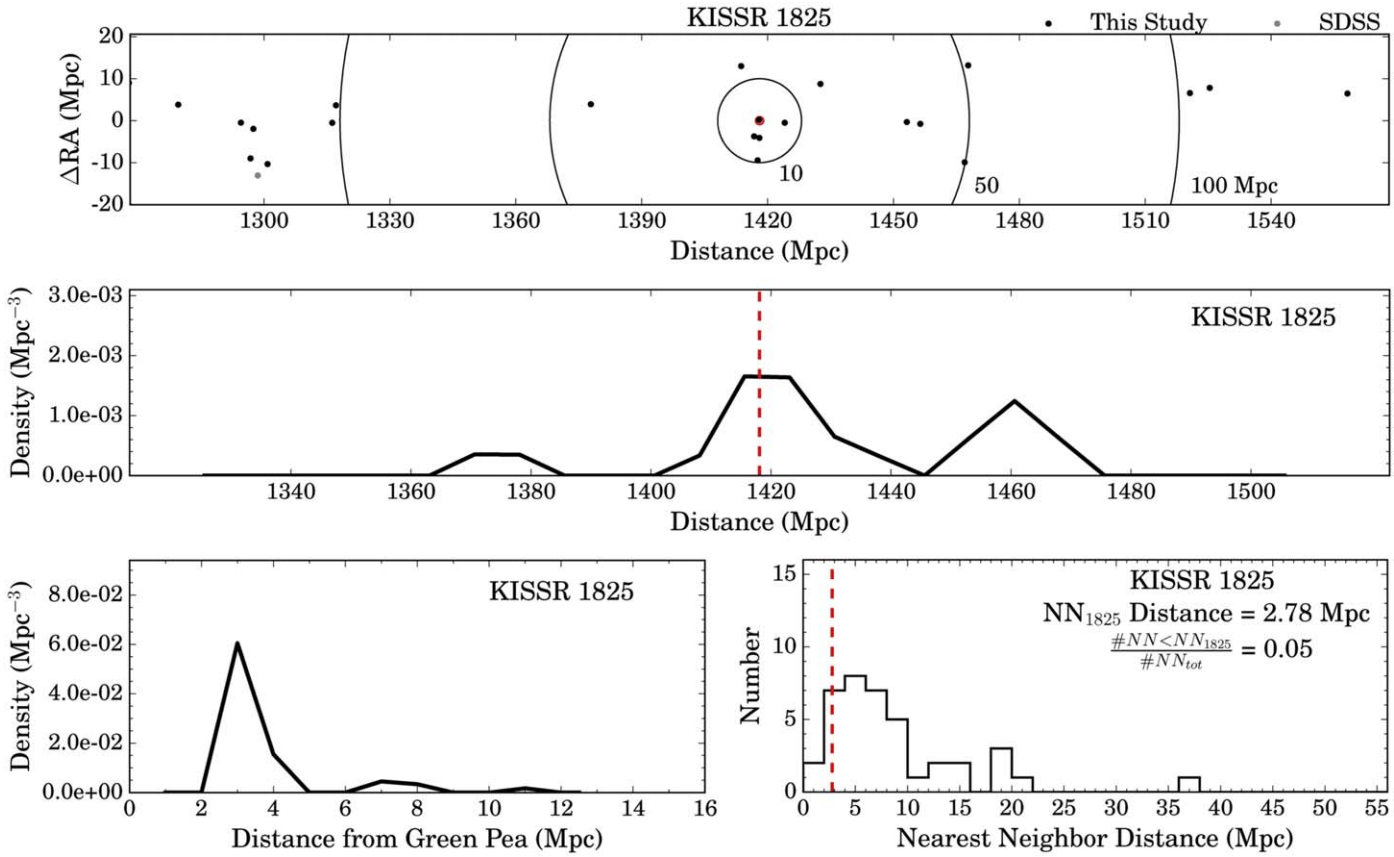

Figure 14. Combined density analysis plots for KISSR 1825. The layout and meaning of the various plots are described in detail in the caption of Figure 5.

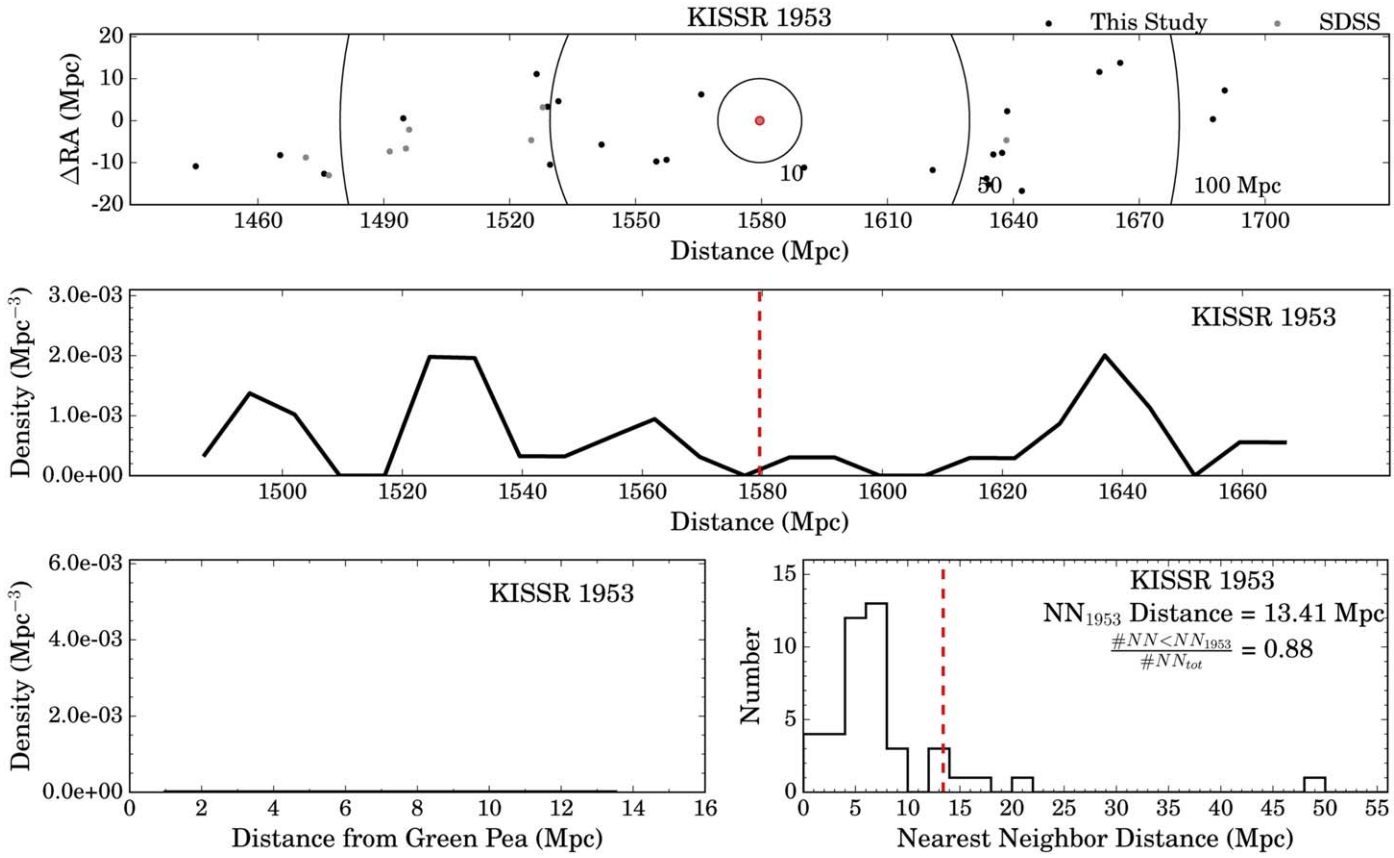

Figure 15. Combined density analysis plots for KISSR 1953. The layout and meaning of the various plots are described in detail in the caption of Figure 5.

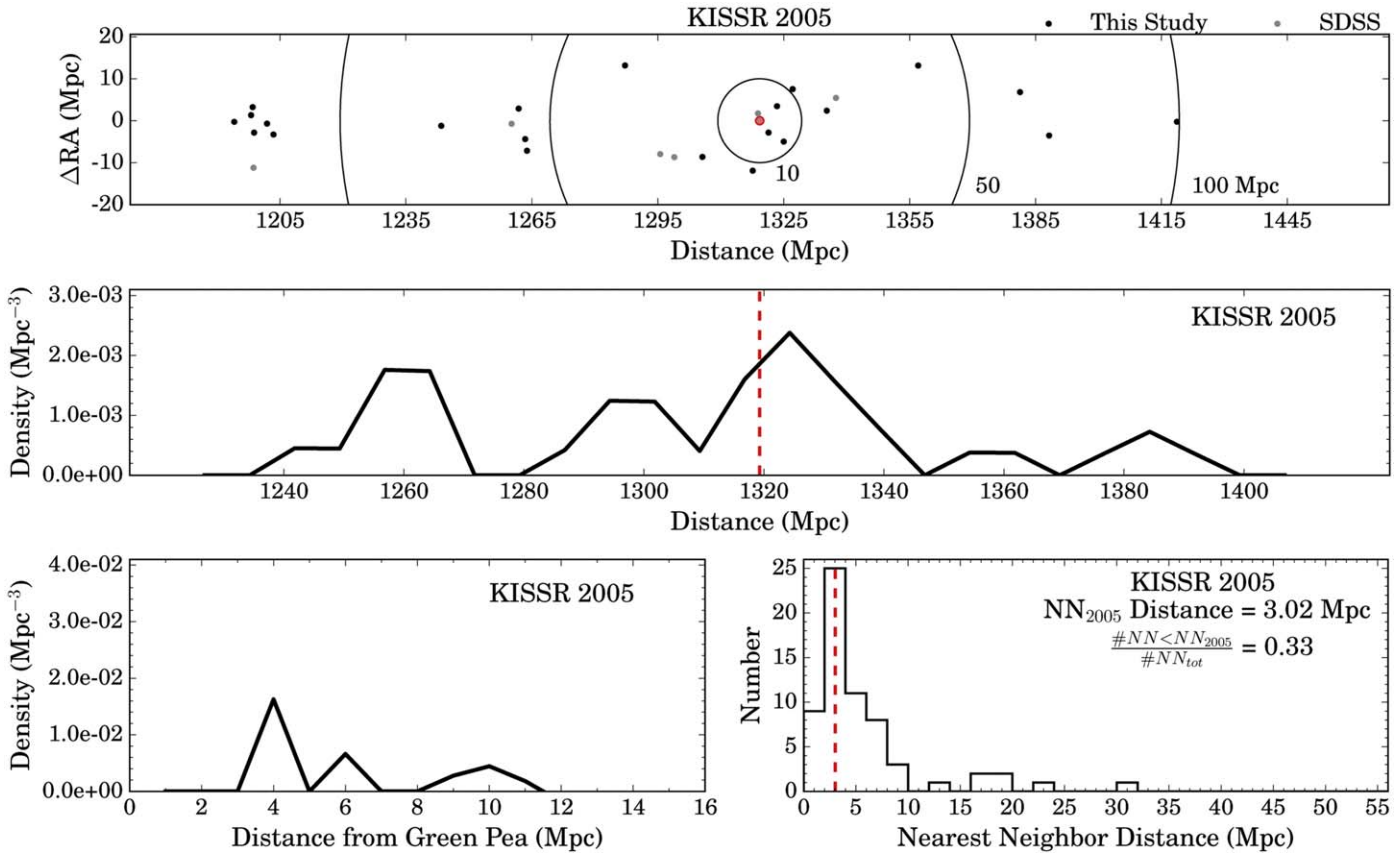

Figure 16. Combined density analysis plots for KISSR 2005. The layout and meaning of the various plots are described in detail in the caption of Figure 5.

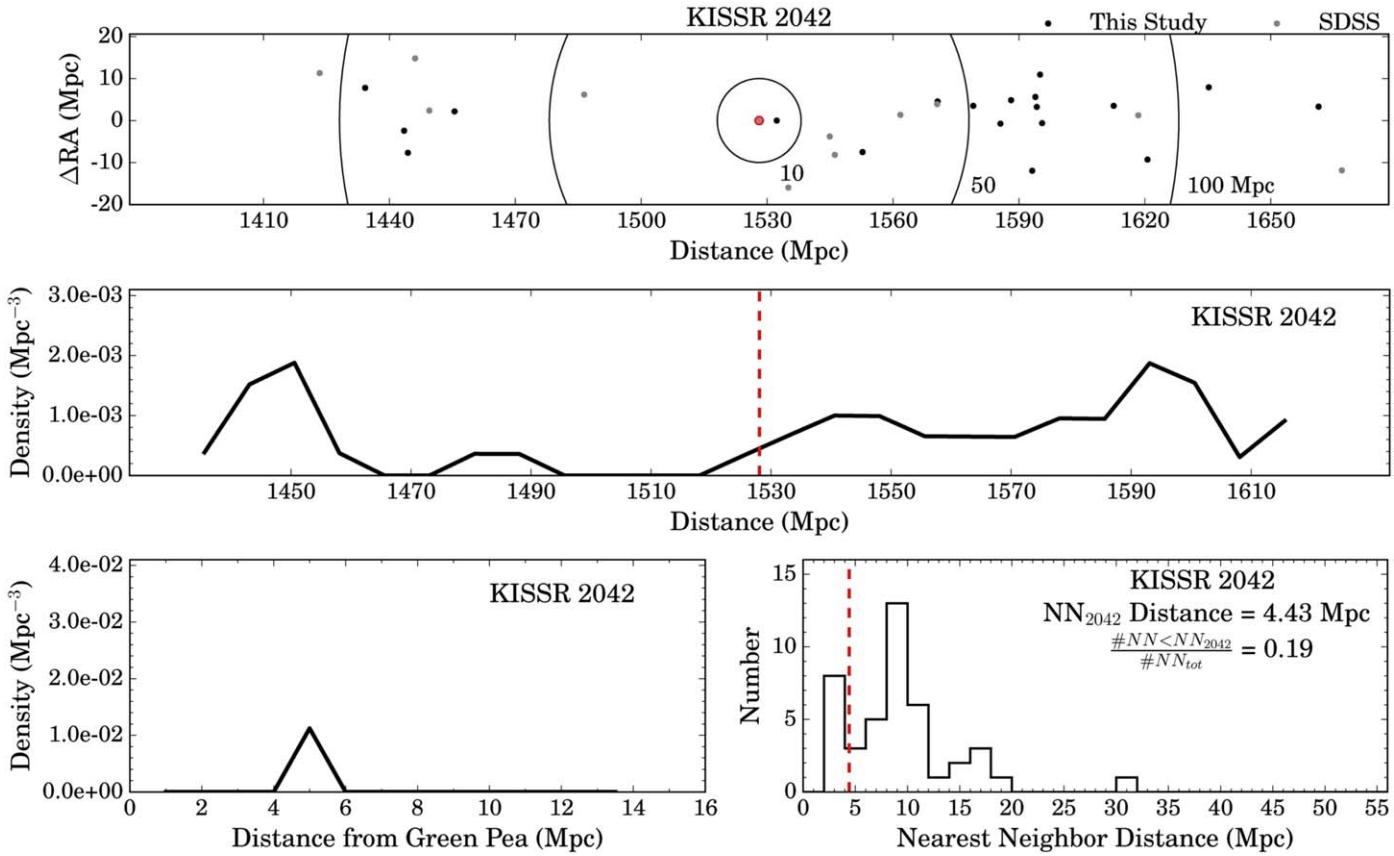

Figure 17. Combined density analysis plots for KISSR 2042. The layout and meaning of the various plots are described in detail in the caption of Figure 5.

its appropriate environment group. Any given parameterization of density calculation is imperfect, so we use four criteria (three density estimators plus the visualization of the environments) to determine which category each GP falls into. This approach combines qualitative and quantitative analyses. While there may be some reasonable debate about which category a specific GP is assigned to, the overall results of our study would not change if these more borderline cases were reassigned to a different category.

4.2.1. Extremely Low-density GP Environments

The GPs located in the extremely low-density environments are perhaps the easiest to identify in our sample. There are 7 in the sample of 13 KISSR GPs that are located in what we classify as extremely low-density environments: KISSR 225, 1038, 1508, 1516, 1791, 1953, and 2042. For these GPs, their nearest-neighbor distances are greater than 4 Mpc, and they are typically not found in a density peak on the 1D density profile for the field. For two of the seven GPs, there is no galaxy within 10 Mpc in our survey. We classify this as an extremely low-density environment because it is essentially void-like. It is highly unlikely that these GPs have had many, if any, major interactions with other $\sim L^*$ galaxies in their lifetimes. This naturally invites us to ask many questions about the formation scenarios for the GPs in these types of environments. It also begs the question about what triggered the intense star formation these GPs are currently experiencing.

4.2.2. Low-density Environments—Tending Toward Isolation

The only GP that we find located in the low-density environment tending toward isolation is KISSR 560. Classifying this type of environment is a little more subjective than the first one. The GP we classified as being in this low-density environment has a nearest neighbor distance of 3.58 Mpc, and it is found in a density peak in the 1D density profile for the field. There are a few galaxies within 10 Mpc of the GP and few more galaxies just outside of that boundary. This is why we feel that this GP environment is still tending toward isolation. A nearest-neighbor distance of 3.58 Mpc is not that close for a neighboring galaxy. Again, the GP in this environment category raises similar questions about the formation and evolution with regard to galaxy interactions as triggers of star formation.

4.2.3. Intermediate-density Environments

The third environment category includes the GPs in the "densest" environments in our survey, though they are still not all that dense. We classify them as intermediate-density environments because they are not nearly as dense as a galaxy cluster or a rich filament would be. There are five GPs that fall within this classification: KISSR 847, 1290, 1759, 1825, and 2005. Several of these galaxies are somewhat close to the boundary of our classifications for low-density and intermediate-density environments, but we have chosen to keep them in the intermediate-density environment category. These GPs have nearest-neighbor distances smaller than 3.5 Mpc, though the smallest nearest-neighbor distance of 1.07 Mpc (KISSR 1290) is still larger than

the Milky Way—M31 separation. There are usually at least four to five galaxies within 10 Mpc of the GP, and the GPs are found near a local peak, sometimes the largest one, in the 1D density profile of the field. These GPs are the ones that have the highest probability of having had an interaction with another galaxy at some point.

4.2.4. Higher-density Environments

We find that none of our sample of 13 KISSR GPs are located within high-density environments such as populous filaments or galaxy clusters. Given the size of our sample, it is possible that this is a result of small number statistics. That is, if the five density categories were evenly populated by our sample, we would expect only 5–6 galaxies in the two highest-density bins. Assuming Poisson statistics apply, the fact that no galaxies are found in these two bins would amount to a $\sim 2.4\sigma$ deviation. However, we interpret it as evidence that GPs do not typically reside in high-density environments.

4.2.5. GPs Found on Edges of Larger Structures

One of the more surprising results from our survey is that we find almost half of the GPs in our sample are located on the edges of larger galaxy structures. A clear example is KISSR 847 shown in Figure 5. One can see in the pencil beam that to the left of the GP (smaller distances) there is a higher density of galaxies, likely part of a filament in the cosmic web, and to the right of the GP (greater distances) there is a void. We find that all of the galaxies in the low-density and intermediate-density environments live on the edges of one of these filament-like structures (i.e., KISSR 560, 847, 1290, 1759, 1825, and 2005). This could be an interesting clue about the formation scenarios for the KISSR GPs. It is possible that the GPs were formed in the voids and are now entering the outskirts of these higher-density filaments for the first time. If this has happened, then it is possible that moving into a higher-density environment could have something to do with triggering the ongoing starbursts in the GPs.

4.2.6. Summarizing the Environment Analyses

We find the KISSR GPs to be located in a range of intermediate- and low-density environments, but we clearly do not find GPs in dense environments like rich filaments or galaxy clusters. We find 8 of the 13 KISSR GPs living in low-density environments, which we further subdivide into two categories of extremely low-density environments and low-density environments tending toward isolation. For these GPs, there is usually no more than one or two galaxies within 10 Mpc, and the GP in this group with the nearest neighboring galaxy is still separated from them by at least 3.6 Mpc. Given the depth of our redshift survey, we cannot entirely rule out galaxy interactions that have occurred with lower-mass galaxies as being a possible trigger for the starburst events in these GPs. However, interactions or mergers seem unlikely to be the main trigger in most cases.

The remaining five KISSR GPs live in slightly higher-density environments, which we have called intermediate-density environments. There are usually around four to five galaxies within 10 Mpcs of these GPs, and their nearest-neighbor distances range from 1.07 to 3.12 Mpc. It is more likely for these GPs to have had an interaction with another galaxy, though it is not necessarily a given that an interaction was the main trigger for their starburst events. We identify which group each GP has been assigned to in column 11 of Table 2. "EI" means the galaxy is found in an extremely isolated or extremely low-density environment, "LD" means the GP was placed in the low-density environment category, and "ID" indicates that the GP belongs to the intermediate-density environment group.

Since we find the majority of GPs in low-density environments, the main question that still remains is what is triggering the intense bursts of star formation currently happening in GPs. The first and possibly easiest solution one would think of, galaxy interactions and mergers, is much less likely to be the answer for GPs. It is possible that some of the GPs were formed in voids and are now entering the edges of larger galaxy structures, and maybe this could be a star formation trigger, though it would not be a solution for all of the GPs in our sample. It is also possible that this starburst event is a typical phase for a GP-like galaxy, and the triggers are internal. We cannot rule out galaxy interactions fully as possible starburst triggers for the GPs as our conclusions only apply to interactions or mergers of galaxies at the luminosity depth of our survey, but we need to start investigating other possibilities for star formation triggers in the GPs based on the outcome of our environment analysis.

4.3. The Impact of Environment on SFR in the KISSR GPs

A fundamental reason for studying the environments of the GPs was to investigate the possible influence the environment has on the GP. Since GPs have such extreme properties, it is natural to consider whether the local environment is directly responsible for the ultra-high SFRs, starburst strengths, and low metallicities. We explore this issue by comparing our measured local densities with a number of key physical properties exhibited by the GPs.

Individually we have shown that the majority of the GPs in the KISSR sample are found in low-density environments, which indicates the environment is likely not the main star formation trigger in these systems. In order to be more quantitative about this comparison, we plotted the densities calculated in the cylindrical density analysis against log(SFR) to see if there was a correlation for the KISSR GPs. This is shown in the left-hand plot of Figure 18. It can be clearly seen that there is no correlation between the density around the GPs and their SFRs. The SFR–density plot is essentially a scatter diagram. If anything, there is a slight tendency for galaxies with the lowest local densities to have *higher* SFRs. Clearly, galaxy–galaxy interactions are not driving the enhanced SF activity in the majority of GPs.

We also compared the densities to stellar mass and metallicity in the center and right-hand plots of Figure 18, respectively. There is no correlation between the densities and those galaxy properties for the GPs either. The same results are found when we compare the GP luminosities and specific SFRs to their densities (not shown). From these comparisons, we find that environments do not have a strong influence on the star formation currently taking place in the KISSR GPs.

5. Conclusions

Green Pea galaxies have stepped into the spotlight in the discussion about star formation and galaxy formation in the early universe. Green Peas are considered low-redshift analogs to the earliest galaxies, but we still lack understanding of what exactly is going on in these extreme galaxies. In this study we carried out a survey of galactic density around 13 KISSR GPs

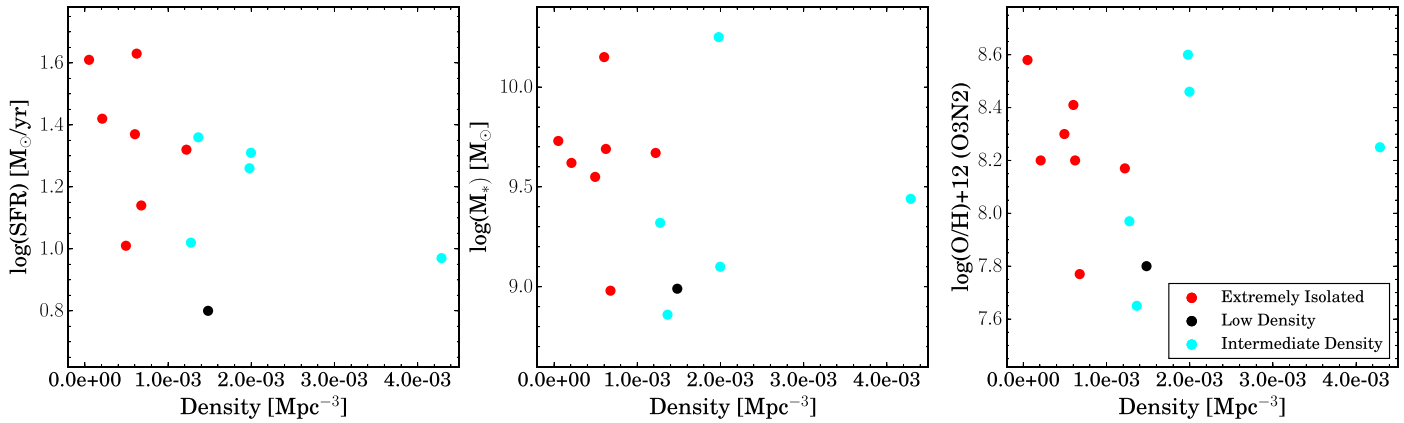

Figure 18. Comparison of the cylindrical densities calculated for each GP field (centered on the GPs) with other properties of the KISS GPs. The red, black, and cyan colored points represent KISSR GPs in the extremely isolated, low-density, and intermediate-density environment categories, respectively. The three plots comparing the densities with SFR, stellar mass, and metallicity are shown in the left, center, and right-hand plots, respectively. They all show essentially the same result: a scatter plot with no correlation between the densities and other galaxy properties for the GPs.

in order to investigate if their star formation is related to their environment. We completed a redshift survey to facilitate this study, and we observed and reduced spectra and measured redshifts for 1312 galaxies distributed between the 13 KISSR GP fields.

In order to study the connection between star formation and environment for GPs, we applied several density analysis methodologies to our redshift survey. The three analysis techniques we used to analyze the galactic densities around the GPs are a cylindrical density analysis, a spherical shell density analysis, and a nearest-neighbor analysis. These density measurement schemes were chosen to match the geometry of our redshift survey. The results of these analyses are presented in a series of plots shown in Figures 5−17.

Based on our analysis, we have discovered that GP galaxies in our sample are found in a range of galaxian environments but with a strong tendency toward low-density environments. We sorted the GPs into one of five environment categories based on the results of our analysis: (1) seven GPs were found to be in extremely low-density environments; (2) one GP was found in a low-density environment, tending toward isolation; (3) five GPs were found in intermediate-density environments; and (4) no galaxies were found in the two higher-density environment categories, such as populous filaments or galaxy clusters. Based on our density analysis and categorization, eight GPs in our sample are found to be very isolated or fairly isolated (the two most isolated categories). Furthermore, most of the five galaxies located in intermediate-density environments are near the edges of local galaxy distributions, on the edges of voids.

After completing the density analysis and categorizing the environments that the GPs in our sample are found in, we directly compared the measured cylindrical densities for each GP (presented in Table 2) with several key physical properties of the GPs. Specifically we wanted to see if the local environment was responsible for the ultra-high SFRs seen in the GPs. These comparisons are shown in Figure 18, and our analysis shows there is no correlation between the key galaxy properties and the galaxian densities.

All of these results strongly suggest that environment is not the dominant factor in driving the activity of the GPs. A caveat to this result is that we do not have a good handle on the most immediate environments around the GPs (i.e., on the few tens of kpc level), so we cannot rule out the possibility that the GPs have had very close interactions with dwarf galaxies.

Kurtz et al. (2016) carried out a similar analysis of GP environments. Their GP sample contained galaxies at the lower-redshift end of the distribution in order to utilize existing SDSS redshift data. They found GPs in a range of different environments, including dense environments like galaxy clusters. This differs from our sample, because we did not find any of the GPs in our sample in higher-density environments.

This study focused on the KISSR GP sample, but we also have another sample of GPs, 16 GPs selected from the Hα Dot survey (Salzer et al. 2000; Kellar et al. 2012), for which we have similarly completed a redshift survey. We will present the same analysis from this study for the Hα Dot GPs in a subsequent paper. When completed, the combined survey will include approximately 2900 new distances to galaxies that previously lacked spectroscopic redshifts.

We are grateful to the Indiana University College of Arts and Sciences for their continued support of the WIYN Observatory. We thank the staff of the WIYN Observatory for their excellent support during our Hydra spectroscopic runs. We acknowledge financial support from the National Science Foundation for the KISS project, as well as for the subsequent follow-up spectroscopy campaign (NSF-AST- 9553020, NSF-AST-0071114, and NSF-AST-0307766). Funding for the SDSS has been provided by the Alfred P. Sloan Foundation, the Participating Institutions, the National Science Foundation, the U.S. Department of Energy, the National Aeronautics and Space Administration, the Japanese Monbu-kagakusho, the Max Planck Society, and the Higher Education Funding Council for England. The SDSS website is http://www.sdss.org/. The SDSS is managed by the Astrophysical Research Consortium for the Participating Institutions. The Participating Institutions are the American Museum of Natural History, the Astrophysical Institute Potsdam, the University of Basel, the University of Cambridge, Case Western Reserve University, the University of Chicago, Drexel University, Fermilab, the Institute for Advanced Study, the Japan Participation Group, Johns Hopkins University, the Joint Institute for Nuclear Astrophysics, the Kavli Institute for Particle Astrophysics and Cosmology, the Korean Scientist Group, the Chinese Academy of Sciences (LAMOST), Los Alamos National Laboratory, the

Max Planck Institute for Astronomy (MPIA), the Max Planck Institute for Astrophysics (MPA), New Mexico State University, Ohio State University, the University of Pittsburgh, the University of Portsmouth, Princeton University, the United States Naval Observatory, and the University of Washington.

Facility: WIYN (Hydra).

ORCID iDs

Samantha W. Brunker https://orcid.org/0000-0001-6776-2550
John J. Salzer https://orcid.org/0000-0001-8483-603X
Bryce Cousins https://orcid.org/0000-0002-7026-1340

References

Baldwin, J. A., Phillips, M. M., & Terlevich, R. 1981, PASP, 93, 5
Barton, E. J., Arnold, J. A., Zentner, A. R., et al. 2007, ApJ, 671, 1538
Barton, E. J., Geller, M. J., & Kenyon, S. J. 2000, ApJ, 530, 660
Blanton, M. R., Hogg, D. W., Bahcall, N. A., et al. 2003, ApJ, 592, 819
Brosch, N., Almoznino, E., & Heller, A. B. 2004, MNRAS, 349, 357
Brunker, S. W., Salzer, J. J., Janowiecki, S., et al. 2020, ApJ, 898, 68
Cardamone, C., Schawinski, K., Sarzi, M., et al. 2009, MNRAS, 399, 1191
Cousins, B. S. 2019, Senior Honors Thesis, Indiana Univ. Department of Astronomy, https://doi.org/10.5281/zenodo.5310770
Gronwall, C., Jangren, A., Salzer, J. J., et al. 2004a, AJ, 128, 644
Gronwall, C., Salzer, J. J., Sarajedini, V. L., et al. 2004b, AJ, 127, 1943
Henry, A., Scarlata, C., Martin, C. L., et al. 2015, ApJ, 809, 19
Hirschauer, A. S., Salzer, J. J., Haurberg, N., et al. 2022, ApJ, 925, 131
Hirschauer, A. S., Salzer, J. J., Janowiecki, S., et al. 2018, AJ, 155, 82
Izotov, Y. I., Guseva, N. G., & Thuan, T. X. 2011, ApJ, 728, 161
Izotov, Y. I., Orlitová, I., Schaerer, D., et al. 2016a, Natur, 529, 178
Izotov, Y. I., Schaerer, D., Thuan, T. X., et al. 2016b, MNRAS, 461, 3683
Izotov, Y. I., Schaerer, D., Worseck, G., et al. 2018, MNRAS, 474, 4514
Izotov, Y. I., Thuan, T. X., & Guseva, N. G. 2017, MNRAS, 471, 548
Jangren, A., Salzer, J. J., Sarajedini, V. L., et al. 2005a, AJ, 130, 2571
Jangren, A., Wegner, G., Salzer, J. J., et al. 2005b, AJ, 130, 496
Jaskot, A. E., Oey, M. S., Scarlata, C., et al. 2017, ApJL, 851, L9
Kellar, J. A., Salzer, J. J., Wegner, G., et al. 2012, AJ, 143, 145
Kennicutt, R. C., Jr. 1998, ARA&A, 36, 189
Kim, K. J., Malhotra, S., Rhoads, J. E., et al. 2021, ApJ, 914, 2
Kurtz, H., Jaskot, A., Drew, P., et al. 2016, AAS Meeting Abstracts, 227, 234.02
Lambas, D. G., Tissera, P. B., Alonso, M. S., et al. 2003, MNRAS, 346, 1189
Li, C., Kauffmann, G., Heckman, T. M., et al. 2008, MNRAS, 385, 1903
Lofthouse, E. K., Houghton, R. C. W., & Kaviraj, S. 2017, MNRAS, 471, 2311
Nakajima, K., & Ouchi, M. 2014, MNRAS, 442, 900
Postman, M., & Geller, M. J. 1984, ApJ, 281, 95
Salzer, J. J., Feddersen, J. R., Derloshon, K., et al. 2020, AJ, 160, 242
Salzer, J. J., Gronwall, C., Lipovetsky, V. A., et al. 2000, AJ, 120, 80
Salzer, J. J., Gronwall, C., Lipovetsky, V. A., et al. 2001, AJ, 121, 66
Salzer, J. J., Gronwall, C., Sarajedini, V. L., et al. 2002, AJ, 123, 1292
Salzer, J. J., Jangren, A., Gronwall, C., et al. 2005, AJ, 130, 2584
Salzer, J. J., Williams, A. L., & Gronwall, C. 2009, ApJL, 695, L67
Veilleux, S., & Osterbrock, D. E. 1987, ApJS, 63, 295
Verhamme, A., Orlitová, I., Schaerer, D., et al. 2017, A&A, 597, A13
Wegner, G., Salzer, J. J., Jangren, A., et al. 2003, AJ, 125, 2373
Wesson, R. 2016, MNRAS, 456, 3774
Yang, H., Malhotra, S., Gronke, M., et al. 2017a, ApJ, 844, 171
Yang, H., Malhotra, S., Rhoads, J. E., et al. 2017b, ApJ, 847, 38
York, D. G., Adelman, J., Anderson, J. E., et al. 2000, AJ, 120, 1579